THE GEOLOGICAL SOCIETY OF AMERICA®

Geochemical, biostratigraphic, and high-resolution geochronological constraints on the waning stage of Emeishan Large Igneous Province

Yuting Zhong[1,†], Roland Mundil[2], Jun Chen[1], Dongxun Yuan[3], Steven W. Denyszyn[4], Adam B. Jost[5], Jonathan L. Payne[6], Bin He[1], Shuzhong Shen[7], and Yigang Xu[1]

[1]*State Key Laboratory of Isotope Geochemistry, Guangzhou Institute of Geochemistry, Chinese Academy of Science, Guangzhou 510640, China*

[2]*Berkeley Geochronology Center, Berkeley, California 94709, USA*

[3]*State Key Laboratory of Palaeobiology and Stratigraphy, Nanjing Institute of Geology and Palaeontology and Center for Excellence in Life and Paleoenvironment, Chinese Academy of Sciences, 39 East Beijing Road, Nanjing 210008, China*

[4]*School of Earth Science, University of Western Australia, Perth WA 6009, Australia*

[5]*Department of Earth, Atmospheric, and Planetary Sciences, Massachusetts Institute of Technology, Cambridge, Massachusetts 02139, USA*

[6]*Department of Geological Sciences, Stanford University, Stanford, California 94305, USA*

[7]*School of Earth Sciences and Engineering, Nanjing University, Nanjing 210023, China*

ABSTRACT

The initiation and peak magmatic periods of the Emeishan Large Igneous Province (LIP) are well constrained by both biostratigraphic and radioisotopic dating methods; however, the age of cessation of volcanism is poorly constrained and continues to be debated. Marine carbonates interbedded with volcanic ashes across the Guadalupian–Lopingian boundary (GLB) are widespread in south China, and these ashes provide an opportunity to study its timing, origin, and potential relationship with the Emeishan LIP. Here we present biostratigraphic constraints, mineralogical and geochemical characteristics, and high-resolution geochronology of ash layers from the Maoershan and Chaotian sections. Stratigraphic correlation, especially conodont biostratigraphy, confines these ashes to the early Wuchiapingian. Those altered ashes are geochemically akin to alkali tonsteins from the coal seams of the lower Xuanwei/Lungtan Formation in southwest China. The ashes postdating the GLB yield a coherent cluster of zircon U-Pb ages with weighted mean $^{206}Pb/^{238}U$ ages of 258.82 ± 0.61 Ma to 257.39 ± 0.68 Ma, in agreement with the ages of intrusive rocks (259.6 ± 0.5 Ma to 257.6 ± 0.5 Ma) in the central Emeishan LIP. Moreover, the $\varepsilon_{Hf(t)}$ values of zircons from the ashes vary from +2.5 to +10.6, a range consistent with that of the Emeishan LIP. The results collectively suggest that the early Wuchiapingian volcanic ashes are a product of extrusive alkaline magmatism and most likely mark the waning stage of the Emeishan volcanism, which may have continued until ca. 257.4 Ma in the early Wuchiapingian.

INTRODUCTION

The Emeishan Large Igneous Province (LIP) in southwest China and northern Vietnam preserves one of the major continental flood basalt eruptions in the Permian (Chung and Jahn, 1995; Xu et al., 2001; Shellnutt, 2014). The volcanic activities associated with the Emeishan LIP magmatism have been extensively studied and are inferred to be connected with the end-Guadalupian biotic crisis (Hallam and Wignall, 1999; Ali et al., 2002; Shen and Shi, 2002; Zhou et al., 2002; He et al., 2007; Wignall et al., 2009; Zhong et al., 2014). The marine Permian stratigraphic records are well exposed and preserved in south China, which makes it an ideal location for investigations related to the Permian biotic crises. Understanding of the end Permian mass extinction has been greatly enhanced in the past three decades, aided by significant progress in high-precision geochronology and high-resolution biostratigraphy (Jin et al., 2000; Mundil et al., 2001, 2004; Shen et al., 2011, 2019a; Song et al., 2013; Burgess et al., 2014, 2015). In contrast, temporal constraints on the end Guadalupian biotic crisis and its potential primary cause—Emeishan LIP magmatism—are relatively poor (Zhou et al., 2002; He et al., 2007, 2010; Wignall et al., 2009; Sun et al., 2010; Shellnutt et al., 2012), and further refinements on the history of the Emeishan LIP magmatism and precise correlation with biodiversity changes in the sedimentary records around the Guadalupian–Lopingian boundary (GLB) are greatly needed to test hypothesized causal connections between volcanism and extinction.

Marine carbonates interbedded with volcanic ash layers across the GLB and in the Lopingian are well preserved and widespread in south China (Zhou, 1999; Zhou et al., 2000; Isozaki et al., 2004; Shen et al., 2010; Dai et al., 2011, 2018; Huang et al., 2018; Shen et al., 2019b), which provides an opportunity to study the age of the sedimentary sequences, the environmental and biological events recorded in the sediments, as well as the origin of the volcanic material and its potential relationship with the Emeishan LIP and/or other regional volcanism. Based on studies at the Chaotian section in northern Sichuan, Isozaki et al. (2004) suggested that a 2-m-thick tuff bed (i.e., the "Wangpo Bed") around the GLB originated from a large-scale explosive eruption with rhyolitic to dacitic composition. The Emeishan volcanism was excluded as the source of the tuff by Isozaki et al. (2004), as acidic components were thought to be lacking in the Emeishan LIP. In contrast, subsequent mineralogical, geochemical, and geochronological studies (He et al., 2007, 2010) indicated that the GLB mudstones of the Chaotian section are not air fall acidic tuff; rather, they are most likely

†zyt9797@gig.ac.cn.

GSA Bulletin; September/October 2020; v. 132; no. 9/10; p. 1969–1986; https://doi.org/10.1130/B35464.1; 13 figures; 4 tables; Data Repository item 2020098. published online 3 February 2020

clastic rocks derived from erosion of the Emeishan LIP. Indeed, various studies (Xu et al., 2010; Shellnutt et al., 2011, 2012; Shellnutt, 2014; Cheng et al., 2017; Hei et al., 2018) have confirmed the volcanic succession of the Emeishan LIP, with low-Ti and high-Ti basalts topped by silicic rocks (e.g., rhyolite, trachyte, and ignimbrite) in the uppermost volcanic sequence (Xu et al., 2010). This silicic component probably represents the final stage of the Emeishan LIP magmatic activity and is similar geochemically to the GLB clay beds (He et al., 2007, 2010; Xu et al., 2010; Zhong et al., 2014). Due to extensive uplift-induced erosion, the majority of silicic constituents, initially located in the uppermost part of the volcanic sequence in the inner zone, have been removed (He et al., 2003), making the exposure of the remnant silicic rocks rather restricted (Xu et al., 2010). Moreover, the Emeishan silicic eruptions are estimated to have been at least ~10^4 km^3 in volume (Yang et al., 2015). Associated release of climatically active gases could have contributed to environmental and biological changes around the Guadalupian–Lopingian transition (Ganino et al., 2008; Xu et al., 2010; Zhang et al., 2013; Yang et al., 2015). Constraining the duration of volcanism and gas release would provide insight on the potential severity of their proximate effects on biota.

Tonsteins are widely distributed throughout the Upper Permian (Lopingian) coal-bearing strata in southwestern China, including western Guizhou, eastern Yunnan, Chongqing, and southern Sichuan (Zhou et al., 1982, 2000; Burger et al., 1990; Dai et al., 2011, 2014a). They are generally considered to be alteration products of volcanic ashes that formed thin and laterally continuous partings within coal beds (Zhou et al., 2000; Dai et al., 2011; Spears, 2012). The geochemistry of these tonsteins indicates an origin from silicic volcanic ash fall (Zhou et al., 1982). Zhou et al. (2000) further suggested that tonsteins in the early stage of the Lopingian were mainly alkaline and that the tonsteins in the middle to upper Lopingian were of silicic and medium-silicic origin. However, the studies mentioned above focused primarily on the spatial distribution, mineralogical, and geochemical characteristics of silicic rocks, tonsteins, and sandstones. Detailed study of their stratigraphy, geochronology, and possible relationship with geological events around the GLB is largely lacking. In addition, the origin of the particular types of altered volcanic ash has not yet been determined.

In this study, we present mineralogical and geochemical data from volcanic ashes around the GLB from the Maoershan and Chaotian sections of south China, constrained with conodont biostratigraphy and high-precision zircon U-Pb geochronology. The comprehensive data set enables us not only to define the characteristics of these volcanic ashes but also to examine their possible source and assess their relationship with Emeishan LIP volcanism. The cause-and-effect relationship between the Emeishan LIP and end-Guadalupian biotic crisis is also briefly discussed.

GEOLOGICAL BACKGROUND

Emplacement of the Emeishan LIP was one of the most prominent geological events during the Middle–Late Permian (Chen and Xu, 2017). The Emeishan LIP consists of flood basalts and contemporaneous mafic–ultramafic intrusions and felsic plutons (Xu et al., 2001; Shellnutt, 2014) that are widely distributed in southwest China (Yunnan, Guizhou, and Sichuan provinces) and northern Vietnam (Song Da zone). Early studies suggested that the Emeishan LIP covers an area of at least 2.5×10^5 km^2 (Xu et al., 2001); more recent investigations (Shellnutt, 2014; Usuki et al., 2015; Li et al., 2017; Liu et al., 2017) have extended the reconstructed areal extent up to ~7×10^5 km^2. The thickness of the Emeishan LIP volcanic sequence varies considerably, from more than 5000 m in the western inner zone to several hundred meters in the eastern outer zone (He et al., 2003, 2007). The entire volume is estimated to range from ~$3–6 \times 10^5$ km^3 (Xu et al., 2001; Shellnutt, 2014) to 3.8×10^6 km^3 (Xu and He, 2007).

Biostratigraphic and geochronological studies (Zhou et al., 2002; He et al., 2007; Sun et al., 2010; Shellnutt et al., 2012; Zhong et al., 2014) indicated that the Emeishan LIP volcanism occurred around the Guadalupian–Lopingian transition. The Emeishan LIP lava succession overlies Guadalupian marine carbonates that are locally known as the Maokou Limestone; these are extensively distributed in south China to form the Yangtze carbonate platform at paleoequatorial latitudes (Wang and Jin, 2000; Shen et al., 2019b). Basinal sedimentary deposits regionally known as the Kuhfeng Formation, which are typified by organic-rich and siliceous-laminated marls and shales, cap the underlying Maokou Limestone (Cao et al., 2018). By the end of Guadalupian time, the Dongwu uplift movement occurred in south China, as indicated by a depositional hiatus with subsequent deposits of terrigenous clastics, coal seams, and ash-clay layers termed the "Wangpo Bed" (Lu, 1956; Isozaki et al., 2004). This distinctive stratigraphic unit reflects the initial stage of Lopingian transgression in south China, overlain by dark gray limestones of the Wuchiaping Formation of Lopingian age (Shen et al., 2019b).

Two stratigraphic successions across the GLB, located in the E'Xi Basin (Maoershan section) and Chuandong Basin (Chaotian section), respectively, are investigated in this study (Fig. 1). The section studied at Maoershan is located ~45 km west of Enshi City, Hubei Province. It consists of a series of small roadside quarries and a large roadside cliff section. The main section (30°20′17.7"N, 109°19′30.7"E) is along National Highway 318 and displays a complete sequence of Capitanian–Wuchiapingian strata. It is nearly 50 m thick, comprising mainly the uppermost Maokou Formation, Kuhfeng Formation, Wuchiaping Formation, and lowermost Talung Formation from bottom to top (Fig. 2). The Maokou Formation consists of massive limestone and dolostone, and only the uppermost part is investigated. The 3.8-m-thick Kuhfeng Formation is composed of thinly bedded black cherts interbedded with thin layers of black shale, which is overlain by the Wangpo Bed, a light gray ash layer ~2 m in thickness with abundant pyrite cubes. The Wangpo Bed is overlain by the Wuchiaping Formation, which consists of thin- to thick-bedded argillaceous lime claystone, wackestone, and packstone. The Talung Formation, a black siliceous shale and chert, overlies the Wuchiaping Formation.

Comparable stratigraphic successions are also well exposed in northern Sichuan Province, including the extensively studied Shangsi section (Shen et al., 2011; Chen et al., 2016; Yuan et al., 2019) and the nearby Chaotian section (32°37′22.8″N, 105°51′36.1″E), the latter of which is investigated in this study (Fig. 1A). The Chaotian section is located ~30 km to the north of Guangyuan, Sichuan Province (Isozaki et al., 2004). The Middle Permian (Guadalupian) to Lower Triassic (Induan) stratigraphic sequence at Chaotian is over 200 m thick, consisting of the Maokou Formation, Wuchiaping Formation, Talung Formation, and Feixianguan Formation from bottom to top (Isozaki et al., 2004, 2007, 2008; Lai et al., 2008; Saitoh et al., 2013a, 2013b). The main part of the Maokou Formation, informally called "Unit 1" in Lai et al. (2008) or "Limestone Unit" in Saitoh et al. (2013a), is composed of thickly bedded to massive, dark gray bioclastic limestone. The upper ~10 m of the Maokou Formation, previously termed "Unit 2" (Lai et al., 2008) or the "Mudstone Unit" (Saitoh et al., 2013a), consists of thinly bedded, dark gray lime mudstone with abundant interbedded cherts, phosphate nodules, and dolomite (Isozaki et al., 2008; Jost et al., 2014). At the top of the Maokou Formation, the black mudstone/chert unit is overlain by the 2-m-thick Wangpo Bed, which is also argued to be made up of erosional products from the felsic member of the Emeishan LIP (He

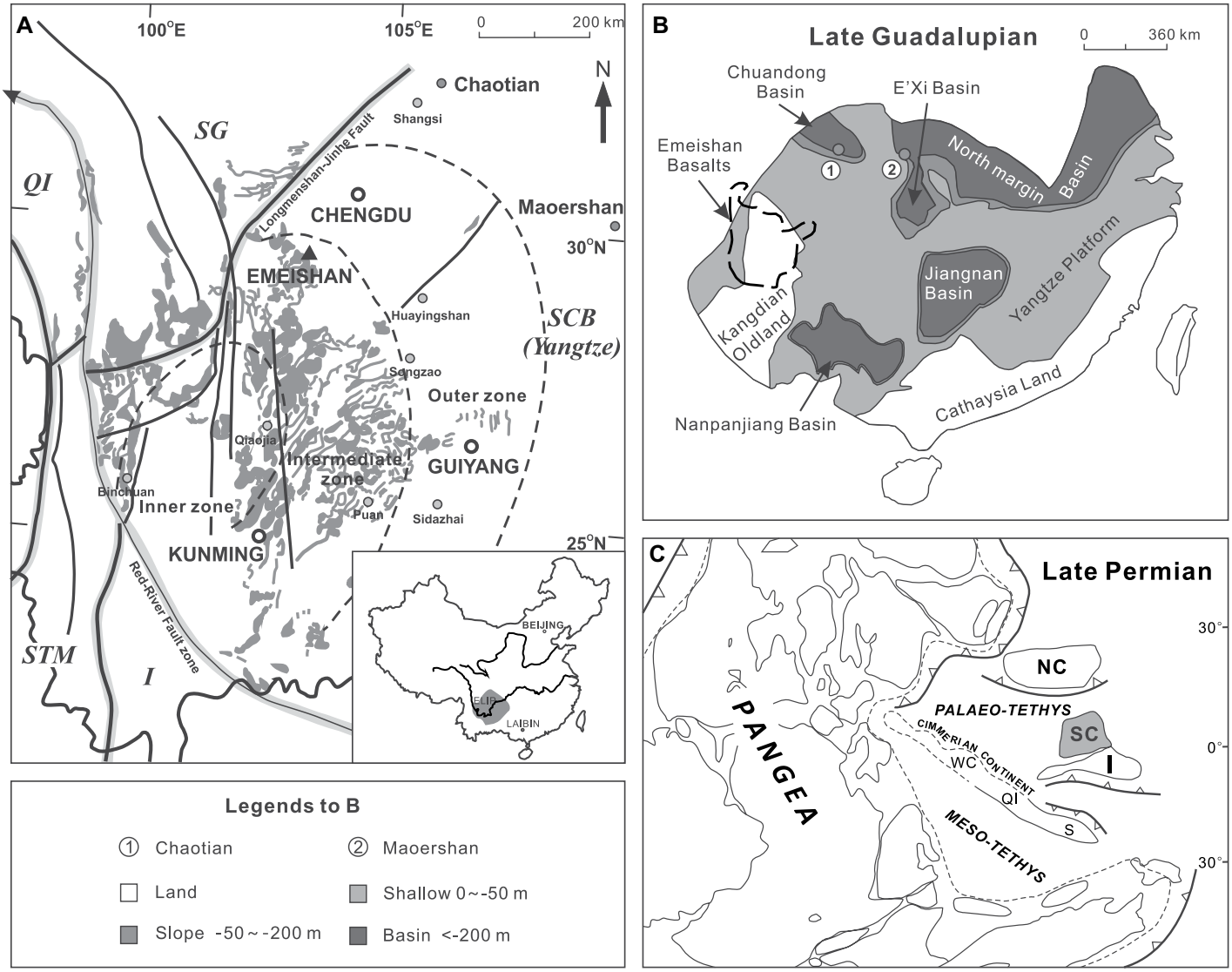

Figure 1. (A) A schematic map showing the Chaotian and Maoershan sections studied and the distribution of the Emeishan Large Igneous Province, modified from He et al. (2007). The dashed lines separate the inner, intermediate, and outer zones, which are defined in terms of extent of erosion of the Maokou Formation (He et al., 2003). SCB—south China block; SG—Songpan-Ganze; QI—Qiangtang; STM—San–Thai–Malay; I—Indochina. (B) Reconstructed paleogeographic map showing the Late Guadalupian isolated basins of the Yangtze Platform in south China, modified from Wang and Jin (2000) and Cao et al. (2018). (C) Global plate reconstruction and position of south China block (SC) in the Late Permian, after Metcalfe (1996). NC—north China; WC—western Cimmerian continent; S—Sibumasu; I—Indochina; QI—Qiangtang.

et al., 2010). The overlying Wuchiaping Formation at this location is ~80 m thick. It begins with a ~1-m-thick calcareous mudstone that is overlain by dark, bituminous limestone and followed by thickly bedded, algal-rich wackestone and packstone containing chert beds and nodules. The uppermost Permian (Changhsingian) to lowermost Triassic (Induan) sequence has been described in detail by Isozaki et al. (2007) and Deconinck et al. (2014). It consists of the Talung Formation, which is composed of siliceous mudstone and organic-rich dark shales and capped by four meters of micritic gray limestone at the top, and the Feixianguan Formation, which consists of thinly bedded, light gray micritic limestone.

MATERIALS AND ANALYTICAL METHODS

To construct a biostratigraphic framework for the strata studied at the Maoershan section, and especially to confirm whether the biostratigraphically defined GLB (i.e., first occurrence (FO) of the conodont *Clarkina postbitteri postbitteri*) is indeed preserved as claimed in previous studies (Wang, 2004; Zhang et al., 2007), a total of 87 conodont samples were collected, covering the interval from 2 m below the top of the Maokou Limestone to 4 m above the base of the Talung Formation (Fig. 2). Each sample weighed between 3 kg and 5 kg. No conodont samples were collected from Chaotian in this study, as previous investigation (Lai et al., 2008) has shown that the Chaotian section can be correlated with the nearby Shangsi section in terms of lithostratigraphic and biostratigraphic successions (Lai et al., 2008; Sun et al., 2010; Yuan et al., 2019). Five conodont zones of the Wuchiapingian were recognized in the Shangsi section, including *Clarkina dukouensis*, *C. asymmetrica*, *C. liangshanensis*, *C. transcaucasica,* and *C. orientalis*, in ascending order

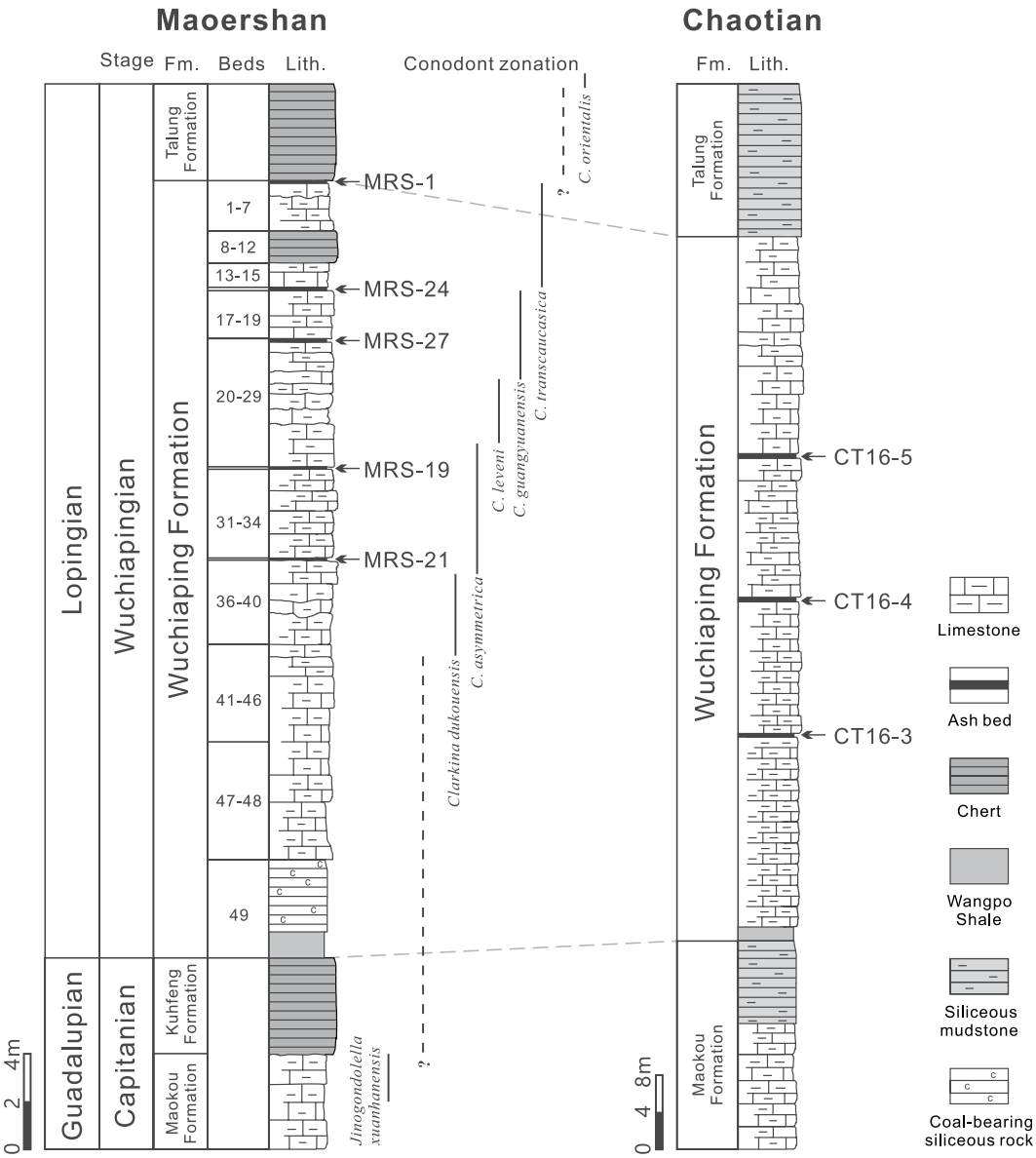

Figure 2. Stratigraphic columns of the Maoershan and Chaotian sections. The conodont biozones at the Maoershan section are indicated.

(Yuan et al., 2019). Processing of conodont samples, extraction, identification, and scanning electron microscope (SEM) photography of conodont specimens was conducted at the Nanjing Institute of Geology and Palaeontology, Chinese Academy of Sciences, following standard procedures (Chen et al., 2011).

Eight volcanic ash samples were collected for mineralogical, geochemical, and zircon U-Pb analyses, including five from Maoershan and three from Chaotian (Fig. 2). Bed subdivisions at the Maoershan section generally follow the scheme of Wang (2004). MRS-1 is at the top of Wuchiaping Formation, which is dark gray in color and 5–10 cm in thickness. MRS-24 was collected from Bed 16 and is pale gray and 3–5 cm in thickness. MRS-27 is interbedded between beds 19 and 20, gray, and 10 cm in thickness. MRS-19 and MRS-21 were collected from beds 30 and 35, respectively, which are very thin (~2 cm). At the Chaotian section, CT16-3, CT16-4, and CT16-5 were collected from ash layers within the Wuchiaping Formation (Fig. 2) located 31.1 m, 45.7 m, and 61.5 m above the top of Maokou Limestone, respectively. All ash beds are pale yellow and ~10 cm in thickness.

Ash samples were analyzed for mineral, major, and trace element compositions at the Guangzhou Institute of Geochemistry, Chinese Academy of Sciences (GIGCAS). Determinations of bulk compositions and clay mineral assemblages were carried out on un-oriented powder mounts by X-ray diffraction (XRD; Bruker D8 Advance). Qualitative and semiquantitative characterization of mineralogy is based on peak intensity measurements of X-ray patterns, and the diagnostic peak and correction intensity factor were obtained for each mineral. The semiquantitative determination of the dominant clay species was based on the height of specific reflections, which were measured on ethylene glycol runs. The intensity of the 10 Å peak was taken as a reference, the other intensities were divided by a weight factor, and all clay species values identified were summed up to 100%. Correction factors were determined by long-term empirical experiments. A pre-ignition was used to determine the loss on ignition (LOI) prior to major element analyses. Major oxides of whole rocks were studied using X-ray fluorescence spectrometry (XRF) on fused glass disks with a Rigaku ZSX-100e XRF instrument. Analytical procedures followed those presented

by Goto and Tatsumi (1996). Trace element concentrations were determined using a Perkin-Elmer Sciex ElAN 6000 inductively coupled plasma–mass spectrometer (ICP–MS) following the techniques described by Li et al. (2002). Analytical uncertainties for major oxides are mostly between 1% and 5%. For rare earth elements (REEs) and other incompatible elements, they are generally better than 5%.

Zircons were separated from six ash samples (MRS-1, MRS-24, MRS-27, CT16-3, CT16-4, and CT16-5) using conventional heavy liquid and magnetic techniques and hand-picking under a binocular microscope. The selected grains were mounted in epoxy and polished down to near half section to expose internal structures. Prior to measurements, samples were documented with transmitted and reflected light micrographs as well as cathodoluminescence (CL) images to reveal their external and internal structures, observe the extent of erosion, and select positions for analyses. U-Pb ages determined by micro-beam analytical techniques were carried out at the State Key Laboratory of Isotope Geochemistry (SKLIG), GIGCAS. Zircon U-Pb dating was conducted by laser ablation–inductively coupled plasma–mass spectrometry (LA–ICP–MS) for the Maoershan samples (MRS-1, MRS-24, and MRS-27) and by secondary ion mass spectrometry (SIMS) for the Chaotian samples (CT16-3, CT16-4, and CT16-5). Subsequently, high-precision zircon U-Pb analyses using chemical abrasion–isotope dilution–thermal ionization mass spectrometry (CA–ID–TIMS) were performed on selected crystals from samples MRS-1, MRS-24, MRS-27, and CT16-5 at the Berkeley Geochronology Center. Analytical details for zircon U-Pb analyses by LA–ICP–MS, SIMS, and CA–ID–TIMS are provided in the Appendix.[1]

Lu-Hf isotopic and trace elements analyses of zircons were conducted on a Neptune Plus multi-collector ICP–MS equipped with a Geolas HD excimer ArF laser ablation system at the Wuhan Sample Solution Analytical Technology Co., Ltd., Wuhan, China. The Lu-Hf isotopic measurements were made on the same spots that were previously analyzed for U-Pb ages. In contrast, in situ U-Pb dating and trace element analyses of zircon were simultaneously conducted on new grains by LA–ICP–MS. Detailed operating conditions for the laser ablation system and the MC–ICP–MS instrument and analytical method are presented in the Appendix.

[1]GSA Data Repository item 2020098, Appendix: analytical methods and Tables A1 and A2, is available at http://www.geosociety.org/datarepository/2020 or by request to editing@geosociety.org.

RESULTS

Conodont Biostratigraphy

The conodont biostratigraphic framework for the Maoershan section places the volcanic ash samples within a clearly defined age framework (Fig. 2), and many of the specimens are well preserved (Figs. 3 and 4). Early studies (Wang, 2004; Zhang et al., 2007) argued that a biostratigraphic GLB, defined by the first occurrence of conodont *Clarkina postbitteri postbitteri* (Jin et al., 2006), can be recognized at Maoershan. Moreover, a complete conodont succession around the GLB, including *Jinogondolella granti*, *Clarkina postbitteri hongshuiensis*, *C. postbitteri postbitteri*, and *C. dukouensis* Zones, has also been reported (Wang, 2004; Zhang et al., 2007). According to the subdivision scheme from Wang (2004), the first occurrence of conodont *Clarkina postbitteri postbitteri* at Maoershan is located at the base of Bed 40, which is a distinct ~1-m-thick massive limestone that can be recognized easily in the field. However, despite intensive sampling around Bed 40, *Clarkina postbitteri postbitteri* was not recovered from Bed 40 in this study. Conodonts are abundant in the uppermost 2 m of the Maokou Limestone and can be assigned to the *Jinogondolella xuanhanensis* Zone. The chert sequence of the Kuhfeng Formation, the volcanic ash layer of the Wangpo Bed, and the coal-bearing siliceous unit of the lowermost Wuchiaping Formation (Bed 49 in Fig. 2) are all unfavorable lithological facies for conodont biostratigraphic study and therefore no samples were collected and their biostratigraphic ages are unknown. Above this unsampled interval, conodont samples were collected systematically from beds 48–41 (Fig. 2). Although conodonts are rare in this argillaceous lime claystone unit, recovered fragments indicate that they belong to the genus *Clarkina*, not *Jinogondolella* as reported in early studies (Wang, 2004; Zhang et al., 2007). In addition, well-preserved specimens from Bed 41 (Fig. 4) demonstrated that this unit is in the *Clarkina dukouensis* Zone, clearly above the GLB when compared with the complete conodont succession in the Penglaitan and Tieqiao sections in the Laibin area, Guangxi (Mei et al., 1998; Jin et al., 2006). Conodonts are common to relatively abundant in the higher parts of the Wuchiaping Formation (i.e., Bed 40-1). Five conodont zones, in ascending order, *Clarkina dukouensis*, *C. asymmetrica*, *C. leveni*, *C. guangyuanensis*, and *C. transcaucasica* Zones, can be recognized. Only one conodont sample was collected from the Talung Formation, which is 4 m above the base of the Talung Formation. This sample contains many *C. orientalis* and a few broken specimens that are like *C. wangi*; therefore, the lower 4 m of the Talung Formation most likely belongs to the *C. orientalis* Zone and is probably near the Wuchiapingian–Changhsingian boundary.

With the conodont biozones established at Maoershan, the biostratigraphic ages of five volcanic ash samples can be assigned, as shown in Figure 2. In ascending order, MRS-21 and MRS-19 are located near the base and top of the *Clarkina asymmetrica* Zone, respectively. MRS-27 is in the middle of the *C. guangyuanensis* Zone, and MRS-24 is around the boundary between the *C. guangyuanensis* and *C. transcaucasica* Zones. The topmost sample, MRS-1, is at the lithological boundary between the Wuchiaping and Talung Formations, which is most likely around the boundary between the *C. transcaucasica* and *C. orientalis* Zones.

Bulk Rock Mineral, Major, and Trace Element Compositions

The samples are mainly composed of clay minerals (illite and montmorillonite, 51.9%–88.2%), with a small amount of other clastic materials (Table 1). MRS-1 and MRS-19 contain abundant quartz and feldspar (38.3% and 31.8%, respectively), whereas three other samples from Maoershan contain minor quartz and feldspar (6.4%–8.6%). Mineral compositions of the Chaotian samples are similar, with illite being the dominant component, accounting for 60.7%–69.4%, while montmorillonite is absent. Each sample also contains some quartz (~13%) and gypsum (3.1%–10.4%).

All samples are characterized by high loss on ignition (LOI) contents (7.68%–14.31%; Table 2), consistent with a high percentage of clay minerals. Also, the high LOI contents indicate that these samples have been heavily weathered and altered. The Zr/TiO_2 versus Nb/Y diagram (Winchester and Floyd, 1977) is used for rock classification because all selected elements are generally considered to remain immobile during alteration/weathering. The samples fall in the field of rhyolite to trachyte (Fig. 5A). In addition, the chemical compositions are characterized by high Al_2O_3 (16.66%–28.58%) and alkalis (up to 5.9% wt. of K_2O) and low MnO (<0.01%–0.02%) and TiO_2 (0.59%–1.14%) contents (Table 2). More specifically, samples MRS-1, MRS-19, and CT16-4 have Al_2O_3 of 16.66%–18.77%, while others have higher Al_2O_3 content (22.49%–28.58%) (Fig. 5B).

The samples have very similar chondrite-normalized rare earth element (REE) patterns (Fig. 6) with enrichment of light REE (LREE) over heavy REE (HREE) and strong negative Eu anomalies ($\delta Eu = 0.12–0.47$).

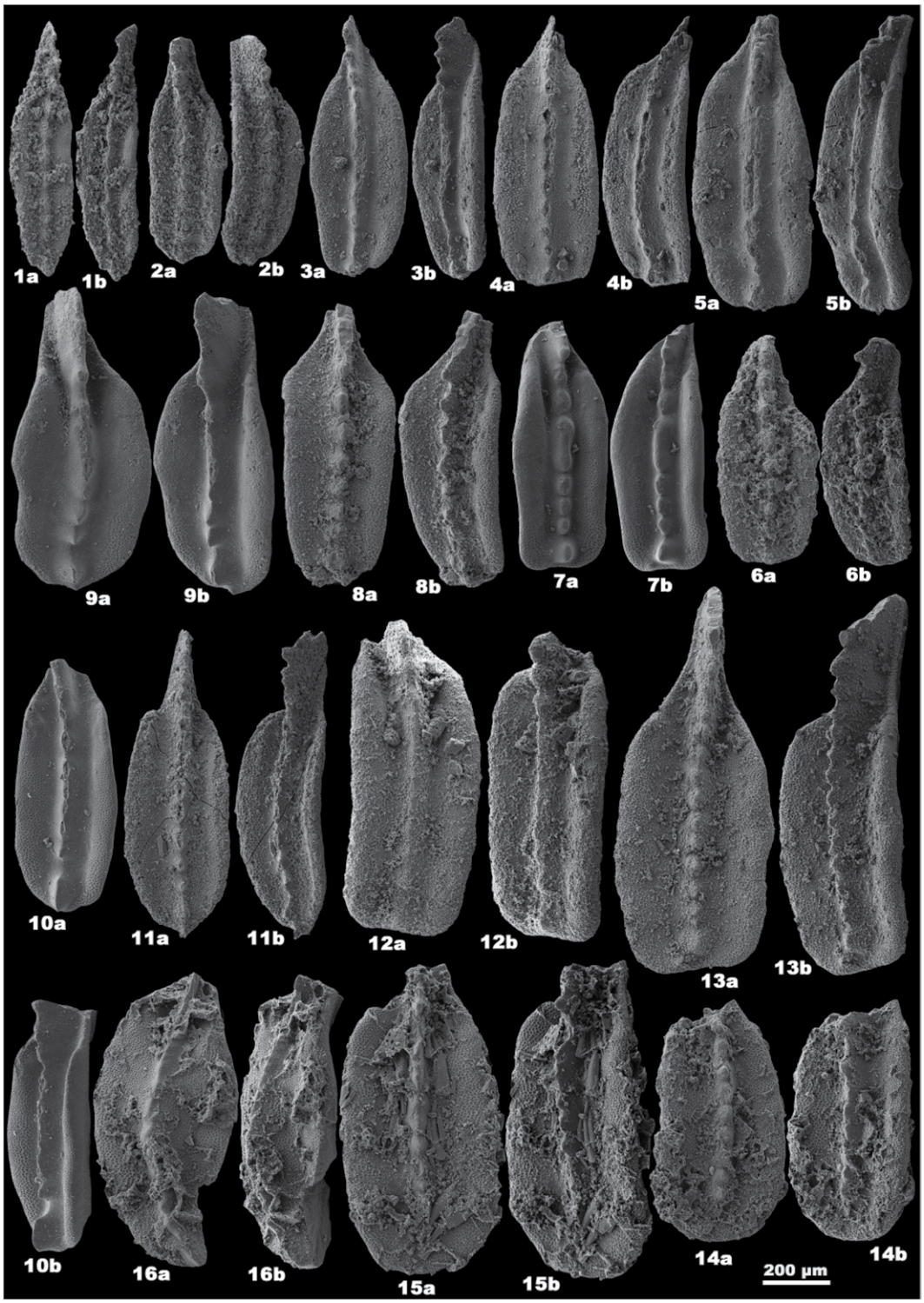

Figure 3. Photomicrographs of representative conodonts from the Maoershan section. (1, 2) *Clarkina dukouensis* Mei and Wardlaw, from Sample Bed 39; (3–5) *Clarkina asymmetrica* Mei and Wardlaw, from Sample Bed 34; (6–8) *Clarkina leveni* (Kozur, Mostler and Pjatakova), 6 from Sample Bed 27; (7–8) from Sample Bed 24; (9–11) *Clarkina guangyuanensis* (Dai and Zhang), from Sample Bed 19; (12–13) *Clarkina transcaucasica* (Gullo and Kozur), from Sample Bed 7; (14–15) *Clarkina orientalis* (Barskov and Koroleva), from Sample Bed 1 + 4 m; (16) *Clarkina cf. wangi* (Zhang), from Sample Bed 1 + 4 m.

Specifically, samples MRS-21, MRS-24, and MRS-27 display more fractionated REE patterns [$(La/Yb)_{CN}$ = 32.7–40.2] than the other five samples [$(La/Yb)_{CN}$ = 7.8–19.7] (Fig. 6). The total rare earth element (ΣREE) content in MRS-1 is 485 ppm, whereas other samples possess significantly higher ΣREE contents of 699–2152 ppm.

Zircon U-Pb Geochronology

Zircon grains are abundant in six samples collected (MRS-1, MRS-24, MRS-27, CT16-3, CT16-4, and CT16-5), enabling precise age determinations. U-Pb isotopic ratios and ages of MRS-1, MRS-24, MRS-27, and CT16-5 that were obtained through the CA–ID–TIMS method are listed in Table 3, and the SIMS U-Pb dating results of CT16-3 and CT16-4 are listed in Table 4. The grains are clear and euhedral, showing oscillatory magmatic zoning in CL images (Fig. 7). Combined with the Th/U ratios (>0.47 for all analyzed zircon crystals), it appears that

Figure 4. Photomicrographs of representative conodonts from the Maoershan section. (1–4) *Clarkina dukouensis* Mei and Wardlaw, 1 from Sample Bed 40-4; 2, 4 from Sample Bed 41-3; 3 from Sample Bed 40-1. (5) *Clarkina sp.*, from Sample Bed 43-2. (6–9) *Jinogondolella xuanhanensis* (Mei and Wardlaw); 6, 7 from Sample MK 0~–30 cm; 8 from Sample MK –165 cm ~–195 cm; 9 from Sample MK –100 cm~–130 cm.

all selected zircons have igneous origins (Hoskin and Schaltegger, 2003).

Sample MRS-1 was collected at the 36.59 m level (top of Maokou Limestone = 0 m) in the Maoershan section (Fig. 2). Nine zircons from sample MRS-1 yield a weighted mean $^{206}Pb/^{238}U$ age of 258.12 ± 0.83 Ma (mean square of weighted deviates (MSWD) = 2.6, n = 8) (Fig. 8A). One crystal was excluded (no. 9) as it gives a significantly younger age than the others; this is interpreted to have resulted from Pb loss. The scatter in excess of the analytical uncertainty may indicate that additional analyses are affected by Pb loss. Excluding them would result in a slightly older age but would require an uncomfortably subjective rejection of data.

Sample MRS-24 was collected at the 32.1 m level in the Maoershan section (Fig. 2). Ten single zircon fragments from sample MRS-24 yield a weighted mean $^{206}Pb/^{238}U$ age of 258.77 ± 0.67 Ma (MSWD = 1.2, n = 9) (Fig. 8A). All fragments are small and thus show relatively low $^{206}Pb/^{204}Pb$ ratios (28–335), resulting in relatively large uncertainties in individual analyses despite sub 1 pg total common Pb concentration in most analyses (Table 3). Analyses no. 3 and no. 10 are notably less precise than the others due to small size and low radiogenic ^{206}Pb. One analysis (no. 10) shows very low $^{206}Pb/^{204}Pb$ ratio, slightly elevated common Pb, and large uncertainty and is therefore excluded.

Sample MRS-27 was collected at the 29.95 m level in the Maoershan section (Fig. 2). Seven single zircon fragments from MRS-27 yield a weighted mean $^{206}Pb/^{238}U$ age of 258.82 ± 0.61 Ma (MSWD = 1.5, n = 6) (Fig. 8A). One datum (no. 1) is excluded from the calculation of the mean as it yields an age slightly older than the rest of the zircon population, which may be due to inheritance.

Sample CT16-5 was collected at the 61.5 m level in the Chaotian section (Fig. 2). Five single zircon fragments from CT16-5 yield a weighted mean $^{206}Pb/^{238}U$ age of 257.39 ± 0.68 Ma (MSWD = 1.3, n = 5) (Fig. 8A).

CT16-3 and CT16-4 were collected at the 31.1 m and 45.7 m levels, respectively

TABLE 1. MINERAL COMPOSITIONS (%) OF THE ASH SAMPLES

Sample number	Illite	Montmorillonite	Quartz	Feldspar	Gypsum	Pyrite	Calcite	Zeolite	Jarosite
Maoershan									
MRS-1	35.2	16.7	19.3	19	6.8	3.1	N.D.*	N.D.	N.D.
MRS-19	52.1	7.8	26.2	5.6	8.3	N.D.	N.D.	N.D.	N.D.
MRS-21	59.7	4.4	3.1	3.8	29.1	N.D.	N.D.	N.D.	N.D.
MRS-24	81.1	6.4	6.4	N.D.	6.1	N.D.	N.D.	N.D.	N.D.
MRS-27	79	9.2	8.6	N.D.	2.6	N.D.	N.D.	0.5	N.D.
Chaotian									
CT16-3	69.4	N.D.	12.6	N.D.	10.4	N.D.	7.7	N.D.	N.D.
CT16-4	60.7	N.D.	13	N.D.	10.4	N.D.	N.D.	N.D.	15.9
CT16-5	69.1	N.D.	13.4	N.D.	3.1	N.D.	14.4	N.D.	N.D.

Note: *N.D. = not determined.

TABLE 2. MAJOR OXIDE (WT%) AND TRACE ELEMENT (PPM) COMPOSITIONS

Sample number	MRS-1	MRS-19	MRS-21	MRS-24	MRS-27	CT16-3	CT16-4	CT16-5
SiO_2	56.95	59.03	48.91	48.85	52.50	51.64	53.77	47.51
TiO_2	0.71	0.63	1.14	0.81	0.99	0.61	0.59	0.84
Al_2O_3	18.55	16.66	28.20	28.58	27.81	23.13	18.77	22.49
Fe_2O_3	4.54	2.32	1.15	1.68	1.33	3.99	3.51	5.33
MnO	0.02	<0.01	<0.01	<0.01	<0.01	0.02	0.01	0.01
MgO	1.51	1.58	2.83	2.73	2.75	3.3	3.79	2.94
CaO	2.84	2.07	1.40	1.68	0.44	2.1	1.57	4.36
Na_2O	0.95	0.55	0.25	0.17	0.18	0.07	0.07	0.05
K_2O	4.28	2.91	4.68	4.71	4.48	5.9	4.91	5.71
P_2O_5	0.81	0.21	0.27	0.25	0.24	0.05	0.02	0.22
L.O.I	8.99	14.31	10.78	10.00	8.60	7.68	10.69	8.85
Total	100.15	100.28	99.61	99.47	99.31	98.49	97.7	98.32
Al_2O_3/TiO_2	26.21	26.57	24.80	35.14	28.13	37.92	31.81	26.77
Sc	17.5	9.392	11.04	8.328	8.056	4.32	3.09	8.11
V	132.1	536.4	211	54.97	31.4	31.2	16.2	132
Cr	115	186.8	64.45	29.83	47.84	15.3	5.28	21.8
Co	19.36	1.566	1.356	1.068	3.587	1.89	0.50	9.53
Ni	210.6	64.56	26.21	22.85	32.46	9.40	2.66	72.5
Cu	162.4	22.56	26.46	16.44	20.52	7.29	5.69	23.1
Zn	176.5	55.36	95.16	62.82	215.4	248	163	430
Ga	18.67	17.09	35.8	29.45	36.91	48.9	55.6	61.5
Rb	146.6	84.1	120.7	116.4	124.9	75.4	79.9	101
Sr	278.8	305.6	203.4	321.9	202.4	120	117	337
Y	115.9	132.8	120.4	109.8	95.63	42.4	95.0	138
Zr	512.7	2373	3488	3301	2615	1859	2444	3219
Nb	42.74	182.3	285.7	211.6	60.87	218	277	342
Cs	7.374	4.247	6.659	5.809	7.012	4.99	6.66	5.40
Ba	354.6	133.1	129.1	96.47	136.1	66.1	282	39.5
La	84.77	263.4	530.2	475.6	463.7	125	142	280
Ce	188.6	520.8	1076	1005	985.4	332	287	586
Pr	22.58	52.63	121.3	108.1	105.8	37.9	32.0	58.1
Nd	91.13	179	286.6	346.2	353.1	143	123	181
Sm	21.72	28.93	31.87	35.93	47.14	26.2	31.4	34.2
Eu	3.379	2.302	1.782	1.508	2.501	2.79	1.80	3.02
Gd	22.31	24.13	39.13	39.31	43.97	17.6	28.4	28.4
Tb	3.767	4.236	5.346	5.602	5.483	2.55	4.45	5.06
Dy	21.89	26.58	29.13	30.33	26.32	12.8	23.9	29.8
Ho	4.172	5.586	5.13	5.254	4.198	2.00	3.87	5.52
Er	10.32	16.59	13.13	13.45	10.33	5.33	10.1	16.7
Tm	1.329	2.605	1.713	1.799	1.383	0.74	1.37	2.37
Yb	7.849	17.32	9.537	10.43	8.272	4.55	8.29	14.6
Lu	1.128	2.661	1.287	1.384	1.114	0.67	1.23	2.21
Hf	14	49.46	93.55	84.06	53.87	44.3	58.4	79.1
Ta	4.487	15.2	29.84	27.72	5.266	13.8	18.0	28.5
Pb	28.62	27.85	27.51	45.26	41.16	31.4	43.9	29.4
Th	19.41	42.26	78.27	77.83	58.21	40.9	40.9	76.5
U	11.65	22.37	12.47	6.549	5.574	3.33	6.12	8.30
∑REE*	484.9	1146.8	2152.2	2079.9	2058.7	713.5	699.3	1246.8
δEu†	0.47	0.26	0.15	0.12	0.17	0.37	0.18	0.29
(La/Yb)CN§	7.75	10.91	39.88	32.71	40.21	19.73	12.29	13.80

*∑REE = total rare earth elements.
†$\delta Eu = EuCN/(SmCN \times GdCN)^{1/2}$.
§CN—Chondrite normalized, normalization values after Sun and McDonough (1989).

(Fig. 2). Fifteen spot analyses of zircons from CT16-3 yield a weighted mean $^{206}Pb/^{238}U$ age of 258.50 ± 2.00 Ma (2σ, MSWD = 0.57; Fig. 8B). Sixteen spot analyses of zircons from CT16-4 yield a weighted mean $^{206}Pb/^{238}U$ age of 258.30 ± 1.90 Ma (2σ, MSWD = 0.76; Fig. 8B). Since the crystals of these two samples are not pretreated with thermal annealing and chemical abrasion, we cannot exclude that the reported ages are slightly too young due to unresolvable Pb loss.

Zircon Trace Elements

All zircons analyzed have similar trace element compositions among the valid data (Table A1, see footnote 1). There is no evident difference between zircons from the Maoershan (Fig. 9A) and Chaotian (Fig. 9B) sections. The zircon grains are all characterized by enrichment in heavy rare earth elements (HREE) with positive Ce anomalies and negative Eu anomalies (Fig. 9), which are typical of magmatic zircons (Hoskin and Schaltegger, 2003). The contents of ΣREE vary in the range of 492–2531 ppm. Y contents vary from 726 ppm to 3557 ppm, and Hf contents are in the range of 7090–10123 ppm. Th contents fluctuate in the range of 28–313 ppm, and U contents are in the range of 55–290 ppm.

The geochemistry of zircons provides a sensitive monitor of its parental magma composition and is effective for fingerprinting tectono–magmatic provenance (Grimes et al., 2015). In general, Nb content of magmatic arc magmas is depleted relative to that of the within plate setting, so that the arc zircons possess lower Nb/Hf and higher Th/Nb ratios. Thus, those ratios are effective for assessing tectonic setting (Yang et al., 2012). All zircons were plotted on the Th/Nb-Hf/Th and Th/U-Nb/Hf diagrams (Fig. 10) to examine the nature of the source magma from which they crystallized (Yang et al., 2012). All data obtained from the Maoershan and Chaotian sections fall into the within plate/anorogenic field (Fig. 10). Data from the upper stratigraphic samples at Shangsi (Huang et al., 2018) and the Permian–Triassic boundary ashes at Meishan (Wang et al., 2019) are also shown in the plots, and they are mainly in the arc-related or orogenic field (Fig. 10).

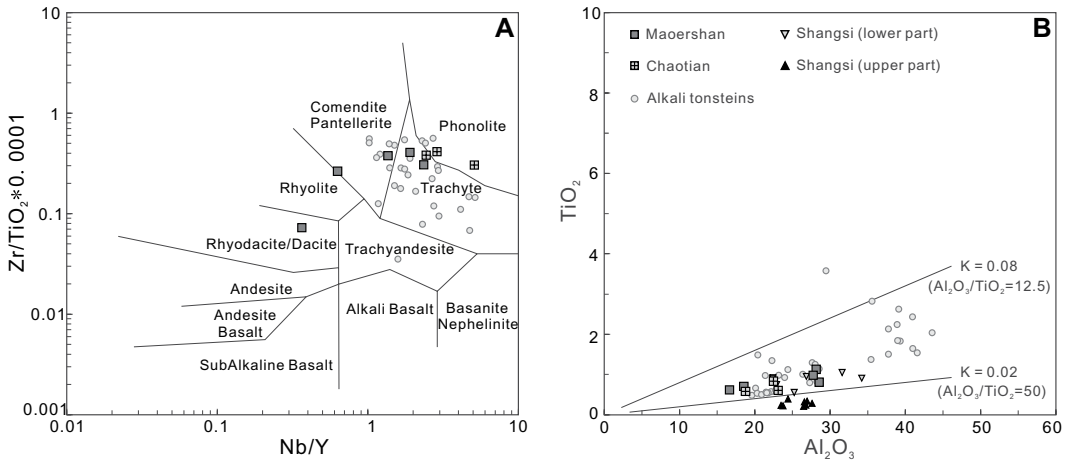

Figure 5. (A) Nb/Y–Zr/TiO_2 classification diagram (Winchester and Floyd, 1977); (B) Al_2O_3–TiO_2 diagram of ash samples from the Maoershan and Chaotian sections. Data of Shangsi section are compiled from Huang et al. (2018); alkali tonsteins data are compiled from Dai et al. (2011), Dai et al. (2014b), and Zhao et al. (2017).

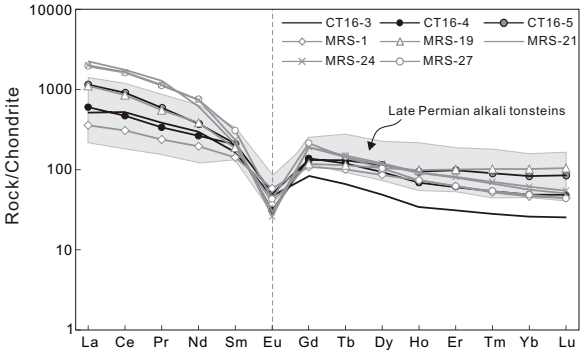

Figure 6. Diagram of Chondrite-normalized rare earth element (REE) patterns for the ash samples from the Maoershan and Chaotian sections; normalization values are after Sun and McDonough (1989). The Late Permian alkali tonsteins data are compiled from Dai et al. (2014b) and Zhao et al. (2017).

Zircon Hf Isotopic Compositions

Ninety-two dated zircon grains (ca. 258 Ma) from five samples (MRS-1, MRS-27, CT16-3, CT16-4, and CT16-5) were selected for in situ Hf isotopic analyses (Table A2, see footnote 1). Twenty spots were analyzed on 20 zircon crystals from sample MRS-1. Zircons display positive $\varepsilon_{Hf(t)}$ values between +2.6 and +7.7 (Fig. 11A) with a weighted mean of 5.65 ± 0.59. Nineteen analyses of MRS-27 exhibit positive $\varepsilon_{Hf(t)}$ values ranging from +3.2 to +9.6 (Fig. 11A) with a weighted mean of 5.90 ± 0.80. Similar Hf isotopic compositions are also observed in the zircons from the Chaotian section. Fifteen, 16, and 22 spots were analyzed on zircon crystals from samples CT16-3, CT16-4, and CT16-5, respectively. They also show positive $\varepsilon_{Hf(t)}$ values (+3.4 to +6.0, +2.9 to +10.6, and +2.5 to +8.3) (Fig. 11A).

ORIGIN OF THE EARLY WUCHIAPINGIAN VOLCANIC ASHES

The Al/Ti ratios of the Maoershan and Chaotian samples suggest an intermediate felsic provenance. As shown in the Al_2O_3 versus TiO_2 diagram (Fig. 5B), all samples fall into the same distribution area with the Late Permian alkali tonsteins (Dai et al., 2011, 2014b; Zhao et al., 2017), indicating that they have similar geochemical compositions. Besides, data of the ash samples from the early Wuchiapingian at the Shangsi section (Huang et al., 2018) are added in the plot and are comparable to our data from Maoershan and Chaotian. In addition, as shown in Figure 6, comparison of the REE patterns of ash samples from Maoershan and Chaotian and the Late Permian alkali tonsteins (Dai et al., 2014b; Zhao et al., 2017) obviously indicates compositional similarity.

Zircons from the Maoershan and Chaotian ash samples exhibit positive $\varepsilon_{Hf(t)}$ values (+2.5 to +10.6), consistent with that of the Emeishan LIP (+0.39 to +13.45) (Xu et al., 2008) (Fig. 11A), indicating a mantle contribution. Furthermore, the zircon U-Pb ages obtained in this study (258.82 ± 0.61 Ma to 257.39 ± 0.69 Ma) are in good agreement with the emplacement age of the intrusive units of the Emeishan LIP (259.6 ± 0.5 Ma to 257.6 ± 0.5 Ma) (Shellnutt et al., 2012). Therefore, the altered volcanic ashes of the early Wuchiapingian collected from the Maoershan and Chaotian sections most likely originated from the extrusive alkaline felsic magmatism of Emeishan LIP.

SEDIMENTARY RECORDS FROM THE WANING STAGE OF EMEISHAN LIP VOLCANISM

The Emeishan LIP occurs at the GLB, whereas the Xuanwei Formation (coal-bearing

TABLE 3. CA–ID–TIMS U-PB ISOTOPIC DATA FOR ZIRCONS FROM MAOERSHAN AND CHAOTIAN SECTIONS

Sample number	common Pb (pg)	Th/U	$^{206}Pb/^{204}Pb$	$^{208}Pb/^{204}Pb$	$^{207}Pb/^{235}U$	2σ (%)	$^{206}Pb/^{238}U$	2σ (%)	ρ†	$^{206}Pb^*/^{238}U$ (Ma)	2σ (abs.)	$^{207}Pb^*/^{235}U$ (Ma)	2σ (abs.)
Maoershan													
MRS-1_1	0.8	0.80	196	82	0.27900	3.63	0.04099	0.37	0.45	258.98	0.96	249.9	9.1
MRS-1_2	1.7	0.51	199	66	0.29208	3.23	0.04094	0.51	0.39	258.67	1.32	260.2	8.4
MRS-1_3	0.9	0.61	272	85	0.29012	3.57	0.04091	0.42	0.46	258.49	1.08	258.7	9.2
MRS-1_4	1.0	0.89	445	156	0.28787	2.08	0.04089	0.31	0.44	258.32	0.81	256.9	5.4
MRS-1_5	1.0	0.54	109	52	0.27539	8.76	0.04068	0.69	0.65	257.02	1.77	247.0	21.6
MRS-1_6	1.0	0.53	555	126	0.29094	1.81	0.04067	1.00	0.61	257.00	2.58	259.3	4.7
MRS-1_7	1.0	0.59	519	130	0.28789	1.51	0.04053	0.80	0.58	256.12	2.04	256.9	3.9
MRS-1_8	3.2	0.53	105	52	0.28135	7.10	0.04053	0.59	0.55	256.11	1.50	251.7	17.9
MRS-1_9	1.2	0.66	553	147	0.28127	1.41	0.04002	0.28	0.34	252.97	0.72	251.7	3.6
MRS-24_1	0.9	0.60	55	44	0.29750	16.11	0.04129	1.29	0.60	260.82	3.36	264.4	42.6
MRS-24_2	0.9	0.68	56	45	0.34229	17.42	0.04117	1.41	0.66	260.09	3.67	298.9	52.1
MRS-24_3	0.9	0.79	33	40	0.38176	34.50	0.04108	3.31	0.68	259.53	8.59	328.3	113.3
MRS-24_4	0.8	0.74	204	80	0.28971	3.47	0.04108	0.48	0.42	259.51	1.25	258.3	9.0
MRS-24_5	1.1	0.61	234	78	0.29162	4.69	0.04103	0.45	0.53	259.23	1.18	259.8	12.2
MRS-24_6	1.0	0.60	79	48	0.30575	11.02	0.04101	0.86	0.64	259.07	2.23	270.9	29.8
MRS-24_7	1.2	0.51	335	87	0.28854	3.07	0.04091	0.33	0.38	258.48	0.85	257.4	7.9
MRS-24_8	0.9	0.76	79	51	0.27776	10.37	0.04085	0.75	0.55	258.07	1.94	248.9	25.8
MRS-24_9	0.8	0.48	91	48	0.24593	12.36	0.04061	0.77	0.73	256.62	1.97	223.3	27.6
MRS-24_10	2.6	0.52	28	39	0.24581	80.22	0.04055	4.90	0.68	256.26	12.55	223.2	179.0
MRS-27_1	2.8	0.76	357	118	0.28417	2.52	0.04140	0.32	0.46	261.48	0.84	254.0	6.4
MRS-27_2	0.8	0.76	163	71	0.29601	4.09	0.04113	0.39	0.54	259.85	1.01	263.3	10.8
MRS-27_3	1.2	0.84	202	85	0.28354	4.41	0.04100	0.38	0.62	259.05	0.98	253.5	11.2
MRS-27_4	1.4	0.75	272	97	0.27803	4.00	0.04100	0.37	0.60	259.03	0.95	249.1	10.0
MRS-27_5	1.0	0.68	181	71	0.28137	4.16	0.04091	0.41	0.52	258.49	1.05	251.7	10.5
MRS-27_6	1.1	0.66	239	82	0.28096	5.10	0.04090	0.40	0.72	258.43	1.02	251.4	12.8
MRS-27_7	0.9	0.69	316	101	0.28717	2.58	0.04088	0.32	0.47	258.26	0.82	256.3	6.6
Chaotian													
CT16-5_1	0.8	0.61	981	221	0.29337	1.57	0.04110	1.14	0.74	259.67	2.95	261.21	4.11
CT16-5_2	1.0	0.55	426	109	0.28513	2.27	0.04076	0.37	0.41	257.56	0.95	254.72	5.78
CT16-5_3	0.7	0.49	963	184	0.28787	0.84	0.04076	0.23	0.40	257.54	0.58	256.88	2.15
CT16-5_4	0.7	0.48	1535	266	0.28052	1.68	0.04064	0.49	0.33	256.80	1.25	251.07	4.21
CT16-5_5	1.1	0.47	799	153	0.28696	1.13	0.04061	0.48	0.51	256.62	1.24	256.16	2.90

Notes: Pb blank composition is $^{206}Pb/^{204}Pb = 18.55 \pm 0.63$, $^{207}Pb/^{204}Pb = 15.50 \pm 0.55$, $^{208}Pb/^{204}Pb = 38.07 \pm 1.56$, and a $^{206}Pb/^{204}Pb$–$^{207}Pb/^{204}Pb$ correlation of +0.9. Present day Th/U ratio is calculated from radiogenic $^{208}Pb/^{206}Pb$ and age. Isotopic ratios are corrected for tracer contribution and mass fractionation (0.15 ± 0.09%/amu). Ratios of radiogenic Pb versus U are corrected for mass fractionation, tracer contribution and common Pb contribution. Uncertainties of individual ratios and ages are given at the 2σ level and do not include decay constant errors. CA-ID-TIMS—chemical abrasion–isotope dilution–thermal ionization mass spectrometry.

*Pb—radiogenic Pb.

†ρ is correlation coefficient of radiogenic $^{207}Pb/^{235}U$ versus $^{206}Pb/^{238}U$.

TABLE 4. SIMS U-PB ISOTOPIC DATA FOR ZIRCONS FROM CHAOTIAN SECTION

Sample number	U (ppm)	Th (ppm)	Th/U	$^{207}Pb/^{235}U$	1σ (%)	$^{206}Pb/^{238}U$	1σ (%)	$^{207}Pb/^{206}Pb$ (Ma)	1σ (abs.)*	$^{207}Pb/^{235}U$ (Ma)	1σ (abs.)	$^{206}Pb/^{238}U$ (Ma)	1σ (abs.)
Chaotian													
CT16-3@02	468	560	1.20	0.2980	1.81	0.0419	1.55	265.3	21.4	264.8	4.2	264.8	4.0
CT16-3@03	134	97	0.72	0.2749	4.00	0.0406	1.50	153.4	84.7	246.6	8.8	256.5	3.8
CT16-3@06	136	82	0.60	0.2984	2.27	0.0415	1.50	291.1	38.4	265.2	5.3	262.2	3.9
CT16-3@07	142	91	0.64	0.2858	2.28	0.0407	1.50	238.4	39.0	255.2	5.1	257.1	3.8
CT16-3@08	118	79	0.67	0.3007	2.68	0.0417	1.56	297.9	48.9	266.9	6.3	263.4	4.0
CT16-3@09	49	23	0.48	0.2914	3.61	0.0406	1.55	288.4	73.0	259.6	8.3	256.5	3.9
CT16-3@10	101	58	0.58	0.2897	3.36	0.0406	1.52	275.1	67.2	258.3	7.7	256.5	3.8
CT16-3@11	109	75	0.69	0.2811	4.62	0.0403	1.60	224.5	97.2	251.5	10.3	254.4	4.0
CT16-3@12	93	51	0.55	0.2954	3.15	0.0413	1.50	281.3	62.1	262.8	7.3	260.7	3.8
CT16-3@13	110	79	0.71	0.2900	2.47	0.0408	1.53	267.8	43.9	258.5	5.7	257.5	3.9
CT16-3@14	133	91	0.68	0.2832	2.64	0.0404	1.63	234.7	47.3	253.2	5.9	255.2	4.1
CT16-3@15	141	97	0.69	0.2908	2.31	0.0408	1.63	270.3	37.1	259.2	5.3	258.0	4.1
CT16-3@16	177	116	0.66	0.2831	3.77	0.0409	1.50	202.6	78.5	253.2	8.5	258.6	3.8
CT16-3@17	172	138	0.80	0.2885	2.27	0.0408	1.76	253.8	32.6	257.4	5.2	257.8	4.4
CT16-3@18	117	66	0.56	0.2960	2.33	0.0408	1.52	311.2	39.7	263.3	5.4	257.9	3.8
CT16-4@01	88	66	0.75	0.3025	3.22	0.0414	1.53	330.8	63.0	268.4	7.6	261.3	3.9
CT16-4@02	62	36	0.59	0.2883	2.94	0.0405	1.55	270.0	56.4	257.2	6.7	255.8	3.9
CT16-4@03	227	173	0.76	0.2890	2.09	0.0406	1.55	270.7	31.9	257.8	4.8	256.4	3.9
CT16-4@04	90	54	0.60	0.2771	5.10	0.0409	1.54	155.5	110.0	248.3	11.3	258.3	3.9
CT16-4@05	75	51	0.69	0.2883	3.14	0.0411	1.61	233.2	61.0	257.2	7.2	259.9	4.1
CT16-4@06	98	71	0.73	0.2879	2.66	0.0407	1.52	252.5	49.3	256.9	6.0	257.4	3.8
CT16-4@07	83	54	0.65	0.2878	3.21	0.0414	1.79	214.1	60.8	256.8	7.3	261.5	4.6
CT16-4@08	88	62	0.71	0.2980	2.21	0.0417	1.53	279.6	36.0	264.8	5.2	263.1	3.9
CT16-4@09	82	49	0.60	0.2918	2.81	0.0402	1.53	310.8	52.8	259.9	6.5	254.3	3.8
CT16-4@10	86	48	0.56	0.2895	2.69	0.0409	1.59	256.7	49.0	258.2	6.1	258.4	4.0
CT16-4@12	97	69	0.71	0.2950	2.15	0.0411	1.51	286.5	34.5	262.5	5.0	259.8	3.8
CT16-4@13	181	128	0.71	0.2906	1.97	0.0402	1.53	301.9	27.9	259.0	4.5	254.3	3.8
CT16-4@14	147	107	0.73	0.2844	2.32	0.0397	1.55	284.0	39.0	254.2	5.2	250.9	3.8
CT16-4@16	441	455	1.03	0.2890	1.74	0.0412	1.51	236.6	19.8	257.7	4.0	260.1	3.8
CT16-4@17	281	156	0.56	0.2930	2.78	0.0417	1.52	241.0	52.7	260.9	6.4	263.1	3.9
CT16-4@18	72	42	0.58	0.2790	3.65	0.0411	1.52	156.9	75.9	249.9	8.1	259.9	3.9

Note: SIMS—secondary ion mass spectrometry.
*abs.—absolute value.

terrestrial clastic rocks) and Lungtan Formation (marine to non-marine transitional series) were deposited around the central Emeishan LIP, namely the Kangdian Oldland (Fig. 1B). Abundant terrigenous materials from the Kangdian Oldland fed into eastern Yunnan and western Guizhou (He et al., 2003), and significant lithofacies changes are present within the Wuchiapingian strata of south China (Shen et al., 2019b). In eastern Guizhou and eastward, terrigenous facies pass laterally into a shallow carbonate platform.

The Late Permian was an important interval of coal formation in southwestern China, especially in eastern Yunnan, western Guizhou, Chongqing, and southern Sichuan. One of the main coal-bearing formations is the lower to middle member of the Xuanwei Formation in eastern Yunnan. It is stratigraphically equivalent to the Lungtan Formation (western Guizhou) and Wuchiaping Formation (eastern Guizhou, eastern Sichuan). Tonsteins, thin and lateral continuous partings in coal beds, are considered airfall volcanic ash layers deposited and altered in a non-marine environment (Bohor and Triplehorn, 1993), and these are well developed in the Late Permian coal-bearing formations mentioned above. Until now, four types of tonsteins, i.e., felsic (Zhou et al., 2000; Dai et al., 2011), mafic (Dai et al., 2011), dacitic (Dai et al., 2014a), and alkali (Zhou, 1999; Zhou et al., 2000; Dai et al., 2011, 2014b) have been identified in coal seams. Remarkably, all alkali tonsteins are only observed in coal beds of the lowest sections of the Xuanwei and Lungtan Formations of southwestern China, equivalent to the earliest Wuchiapingian stage. Evidence shows that the alkali tonsteins from southwest China originated from coeval Emeishan LIP alkaline magmatism. Dai et al. (2011) tentatively suggested that the alkaline tonsteins in Chongqing may have been derived from waning activity of the Emeishan mantle plume; Dai et al. (2016) argued that the late stage volcanism and hydrothermal activities induced by impingement of the mantle plume served as the source of tonsteins and nanoquartz present within the Upper Permian coal seams of southwest China. Zhao and Graham (2016) and Dai et al. (2018) reached a similar conclusion that the enrichment of Nb-Zr-REE-Ga in alkali tonsteins occurred because they originated from Emeishan LIP alkaline Nb-Ta-enriched volcanic ashes and may represent the last stage of mineralization associated with Emeishan mantle plume activity. Nevertheless, it remains unclear whether this model explains the origin of other contemporaneous deposition during the early Wuchiapingian of south China.

On the other hand, an Emeishan LIP-related drowning event (Mapojiao event, southern Guizhou) during the early Wuchiapingian is thought to represent the youngest burst of Emeishan LIP eruptive activity (Bagherpour et al., 2018a, 2018b). Carbon isotope compositions of carbonates ($\delta^{13}C_{carb}$) document a new 3.5‰ carbon isotope excursion (CIE) toward lower values concomitant with the event (Bagherpour et al., 2018a). Additionally, Lopingian volcanic ashes at the Shangsi section (Guangyuan, northeastern Sichuan) were geochemically investigated by Huang et al. (2018). They concluded that the older ash horizons were sourced from the Emeishan LIP based on the trace elemental and Lu-Hf isotopic compositions of zircons, which are consistent with the climate cooling event recorded in the early Wuchiapingian (Yang et al., 2018).

The Th/Sc ratio is a useful indicator of source rocks and is unaffected by sedimentary processes (McLennan et al., 1993). It is thought to be the most sensitive indicator of the bulk composition of the provenance source rock. Besides that, the Zr/Sc ratio is an index of zircon enrichment. The samples present an approximately linear distribution in the Zr/Sc-Th/Sc plot (Fig. 12), which illustrates the compositional variation of Emeishan LIP rocks. In this space, the ash samples correspond to alkali tonsteins of the early Wuchiapingian. In contrast, the ash layers from the upper part of the Shangsi section do not. In summary, these volcanism-related deposits, distributed in the inner, intermediate, and outer zones as well as beyond the defined margins of the Emeishan LIP, represent a sedimentary record for the waning stage of Emeishan volcanism in south China. As demonstrated in Figure 13, the sedimentary record of alkaline volcanism is recorded across southwest China as would be expected from volcanogenic tuff deposition that represents the waning stage of Emeishan plume activity.

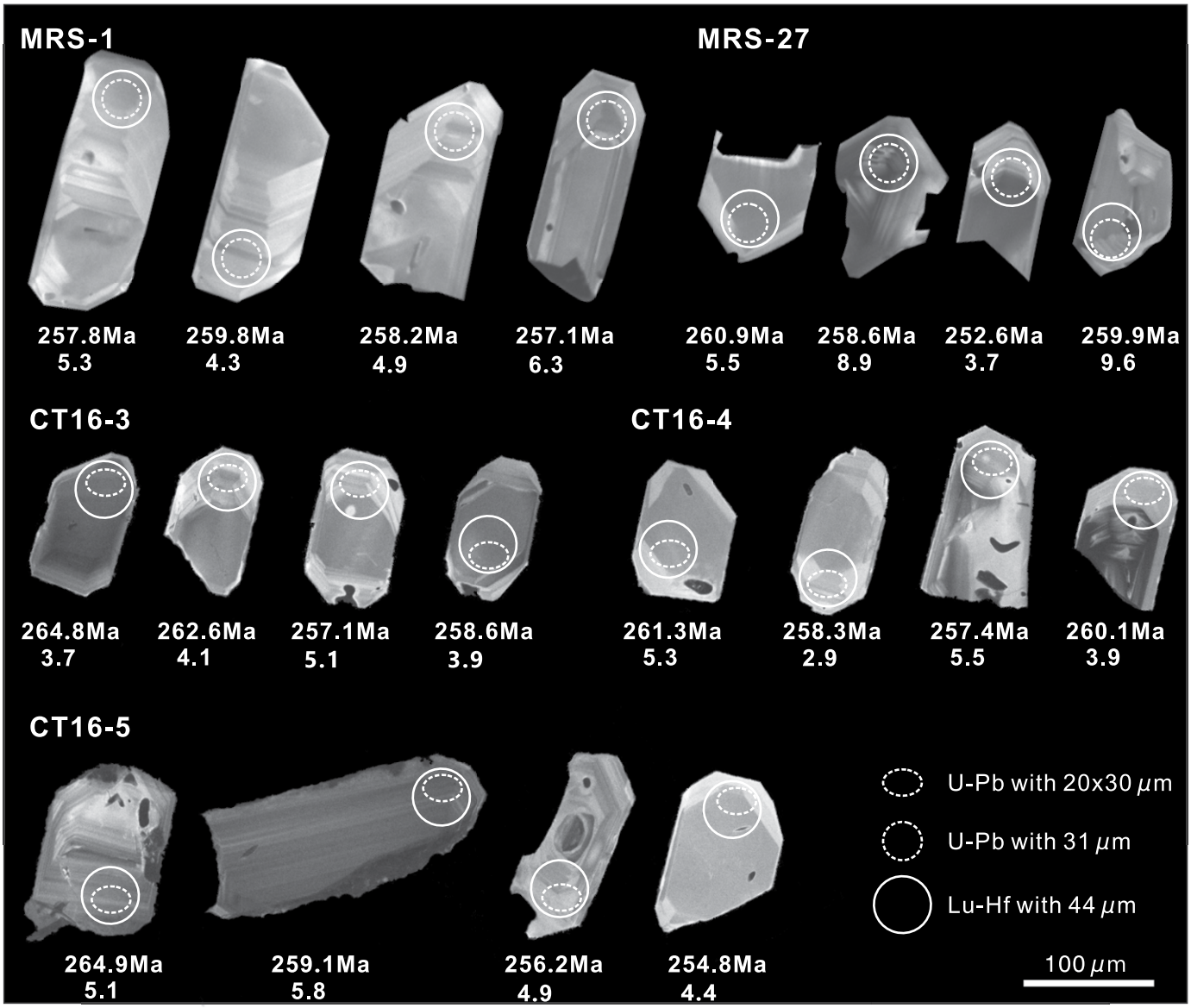

Figure 7. Representative cathodoluminescence (CL) images of zircons from the Maoershan and Chaotian sections. The numbers below each grain are $^{206}Pb/^{238}U$ age and corresponding $\varepsilon_{Hf(t)}$ values, respectively.

AGE CONSTRAINTS ON THE DURATION OF EMEISHAN LIP VOLCANISM

According to Bryan and Ernst (2008), recognizing the initial phase of LIP magmatism is more straightforward than identifying its terminal phase. This asymmetry applies perfectly to the Emeishan LIP, the onset of which is well constrained by both biostratigraphic and radioisotopic techniques, whereas the age of cessation of magmatism is unclear and continues to be debated (Shellnutt, 2014; Bagherpour et al., 2018b). Sedimentology and biostratigraphy constrain the eruption of the Emeishan LIP to the late part of the Middle Permian (He et al., 2007; Sun et al., 2010). Sun et al. (2010) demonstrated that eruptions began in the *Jinogondolella altudaensis* Zone (ca. 263 Ma) within the middle of the Capitanian stage and greatly increased in extent and volume in the *J. xuanhanensis* Zone (ca. 262 Ma).

Early attempts to radioisotopically date the voluminous basalt units of the Emeishan LIP directly using the $^{40}Ar/^{39}Ar$ method were unsuccessful due to highly disturbed age spectra and overprint ages resulting from Mesozoic and Cenozoic regional tectonic events (Boven et al., 2002; Lo et al., 2002; Ali et al., 2004). However, very fresh samples discovered at the base of the high-Ti basalt sequence at Qiaojia County yielded an accurate $^{40}Ar/^{39}Ar$ age of 260.1 ± 1.2 Ma, marking the onset of the high-Ti volcanism of the Emeishan LIP (Li et al., 2018). On the other hand, due to the limited resolution, ages determined by microbeam analytical techniques (i.e., SIMS and LA–ICP–MS) have constrained the intrusive magmatism of the Emeishan LIP as contemporaneous with the Capitanian–Wuchiapingian boundary and extend the duration of magmatism to ~10 m.y. (Shellnutt et al., 2012). The first high-precision zircon CA–ID–TIMS geochronology results from a suite of diabase dykes and granitic rocks that yielded ages tightly clustered between 257.6 ± 0.5 Ma and 259.6 ± 0.5 Ma, constraining the magmatism in the Emeishan LIP to an interval from ca. 257 Ma to 260 Ma (Shellnutt et al., 2012). Zhong et al.

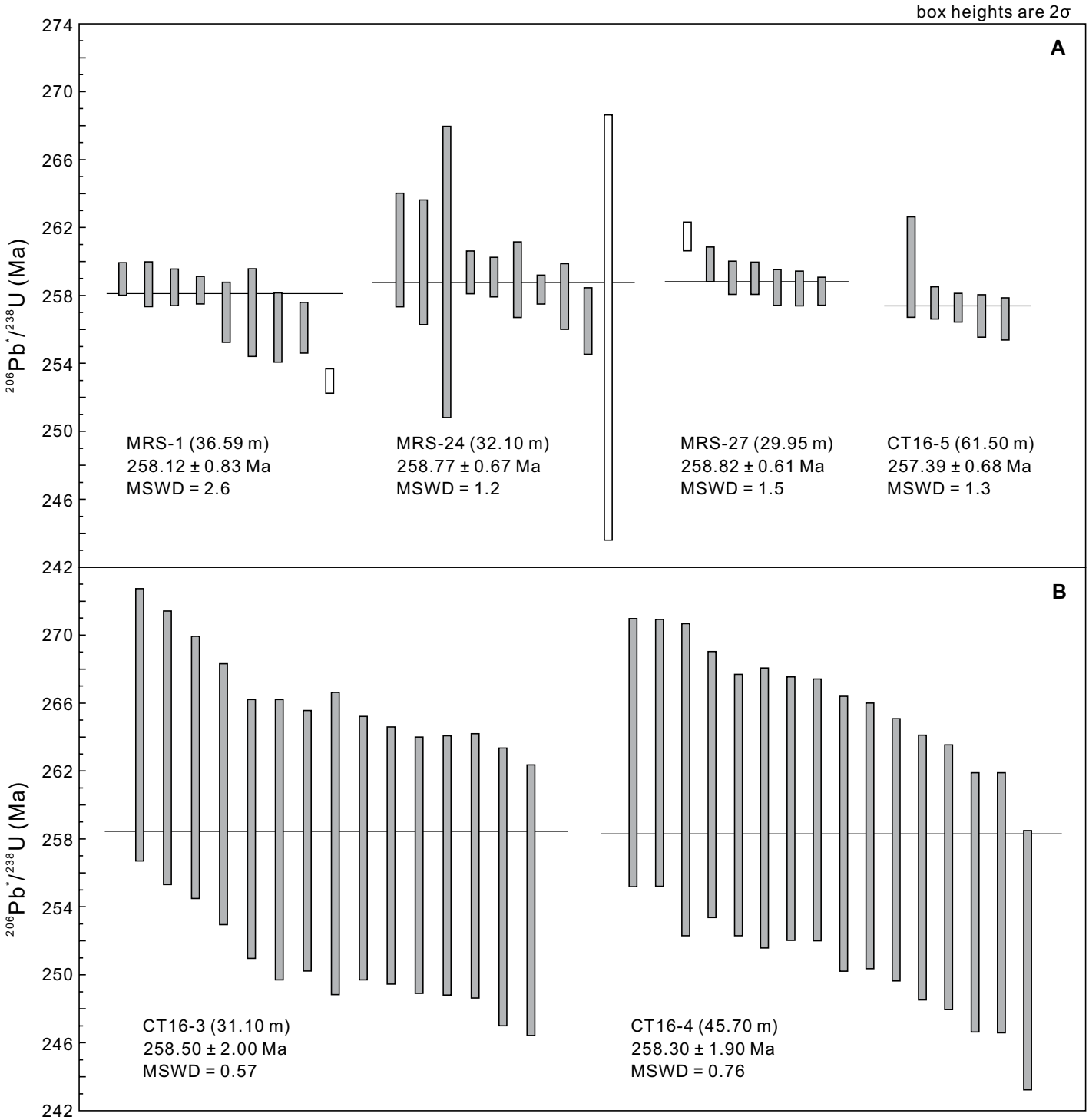

Figure 8. Ranked age plots for individual analyses yielding a weighted mean $^{206}Pb/^{238}U$ age for samples (A) MRS-1, MRS-24, MRS-27, and CT16-5, as analyzed by the high-precision chemical abrasion–isotope dilution–thermal ionization mass spectrometry (CA–ID–TIMS) method; and (B) samples CT16-3 and CT16-4, as analyzed by secondary ion mass spectrometry (SIMS). MSWD—mean square of weighted deviates.

(2014) obtained a U-Pb age of 259.1 ± 0.5 Ma for zircons from the felsic ignimbrite at the top of the flood basalt lava succession at Binchuan, Yunnan. Thus, the main episode of Emeishan flood basalt volcanism most likely terminated at 259.1 ± 0.5 Ma (Zhong et al., 2014). The top tuff from the Pu'an volcanic succession yielded an age (259.51 ± 0.21 Ma) identical within error to that of the Binchuan ignimbrite (Yang et al., 2018).

According to Huang et al. (2018), the Lopingian volcanic ashes from the lower strati-

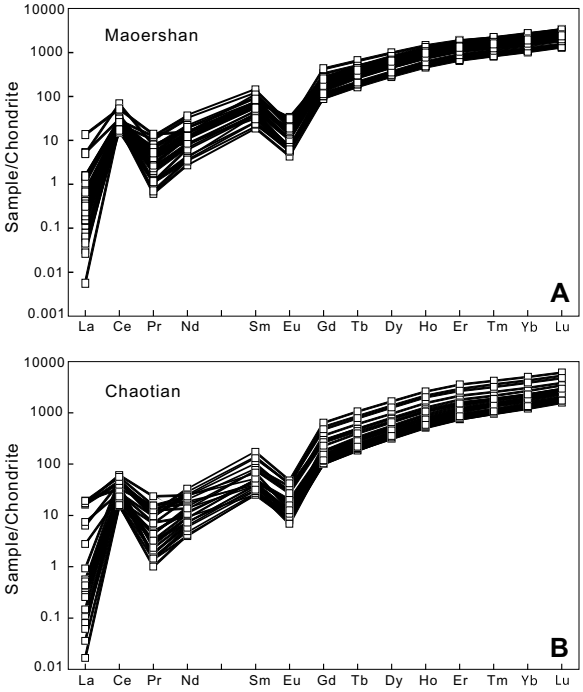

Figure 9. Chondrite-normalized rare earth element (REE) patterns for zircons from the (A) Maoershan and (B) Chaotian sections. Normalization values are after Sun and McDonough (1989).

graphic succession of the Shangsi section originated from felsic volcanism related to the Emeishan LIP. Zircons from their studied ash layer (P6–1 of Bed 15; 257.79 ± 0.14 Ma) (Shen et al., 2011) exhibit positive $\varepsilon_{Hf(t)}$ values (+4.7 to +14.2; Huang et al., 2018). Zircons from the upper stratigraphic samples have lower $\varepsilon_{Hf(t)}$ values ranging from –4.9 to +2.2 and entirely different Th/Nb values than the lower stratigraphic samples (Fig. 11). Combined with the high-precision CA–ID–TIMS data obtained in this study, we conclude that the waning stage of the Emeishan felsic volcanism may have lasted until ca. 257.4 Ma in the early Wuchiapingian. Additionally, sample MRS-1 (258.12 ± 0.83 Ma) was collected near the boundary between the *C. transcaucasica* and *C. orientalis* Zones (Fig. 2). The result also could correlate with those from the Mapojiao and Shangsi sections (Shen et al., 2011; Bagherpour et al., 2018b), corresponding to an absolute age of ca. 258 Ma (Ogg et al., 2016).

More significantly, it is well displayed in the evolution of SW China, where the competing influences of the plume-induced Emeishan LIP and orogeny-induced tectonic events occur along a series of Palaeotethyan suture zones (eg., Metcalfe, 2011; Sone and Metcalfe, 2008; Jian et al., 2009; Lin et al., 2012; Zi et al., 2013; Wang et al., 2018). As stated above, the disparate geochemical behavior of Hf, Th, and Nb in zircon provides a potential scheme for the tectonic setting discrimination of the primary magma (Yang et al., 2012). Nb in arc magmas is strongly depleted compared to that of within-plate magmas (Sun and McDonough, 1989; Pearce and Peat, 1995). It follows that the arc zircons possess lower Nb/Hf and higher Th/Nb than those from within-plate settings at a comparable degree of magmatic fractionation (illustrated in Figs. 10A, 10B, and 11B). Meanwhile, the positive $\varepsilon_{Hf(t)}$ values of zircons from the Emeishan LIP indicate a dominant mantle contribution, while the overwhelmingly negative $\varepsilon_{Hf(t)}$ values are observed in arc-related zircons (Fig. 11A). Therefore, the distinct change for provenance interpretation (Fig. 11) indicates tectonic switching in the source region from the Emeishan LIP to subduction-related magmatism from ca. 257 Ma to 255 Ma.

Mainly based on the proposed temporal linkage, it is increasingly thought that the volcanic and intrusive activities related to the Emeishan LIP might be ultimately linked with many of the purported proximal kill mechanisms leading to the end-Guadalupian biotic crisis (e.g., Zhou et al., 2002; He et al., 2007; Wignall et al., 2009; Bond et al., 2010; Xu et al., 2010; Zhang et al., 2013). Thus, constraining the timing and duration of Emeishan LIP magmatism is central to testing its link to the biotic crisis. Therefore, high-precision geochronology is obviously pivotal in testing a potential between LIP volcanism and environmental and biological changes, which means that ideally the history of LIP eruptions, environmental changes recorded in the marine and terrestrial realms, and biodiversity changes should be correlated in a unified, high-precision temporal framework (Chen and Xu, 2019). Based on the Permian timescale (Henderson et al., 2012; updated by Shen et al., 2019b) and the complete conodont succession of the Penglaitan–Tieqiao sections in Guangxi (Mei et al., 1998; Jin et al., 2006; Sun et al., 2017), the suggested earliest eruption and peak ages from Sun et al. (2010) can be recalculated to ca. 263.5 Ma and 260.9 Ma, respectively (Chen and Xu, 2017). In summary, we suggest that the main

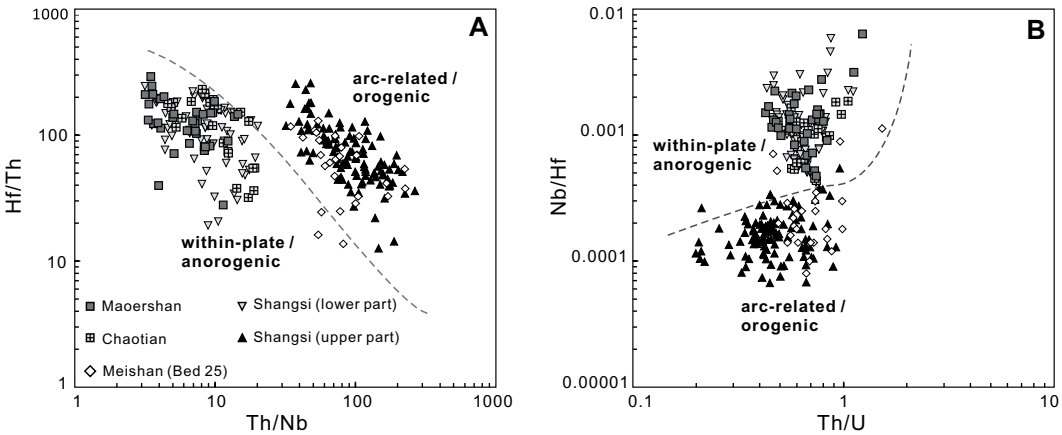

Figure 10. (A) Th/Nb–Hf/Th and (B) Th/U–Nb/Hf diagrams for zircons from the Maoershan and Chaotian sections. Data from Shangsi and Meishan are compiled from Huang et al. (2018) and Wang et al. (2019), respectively.

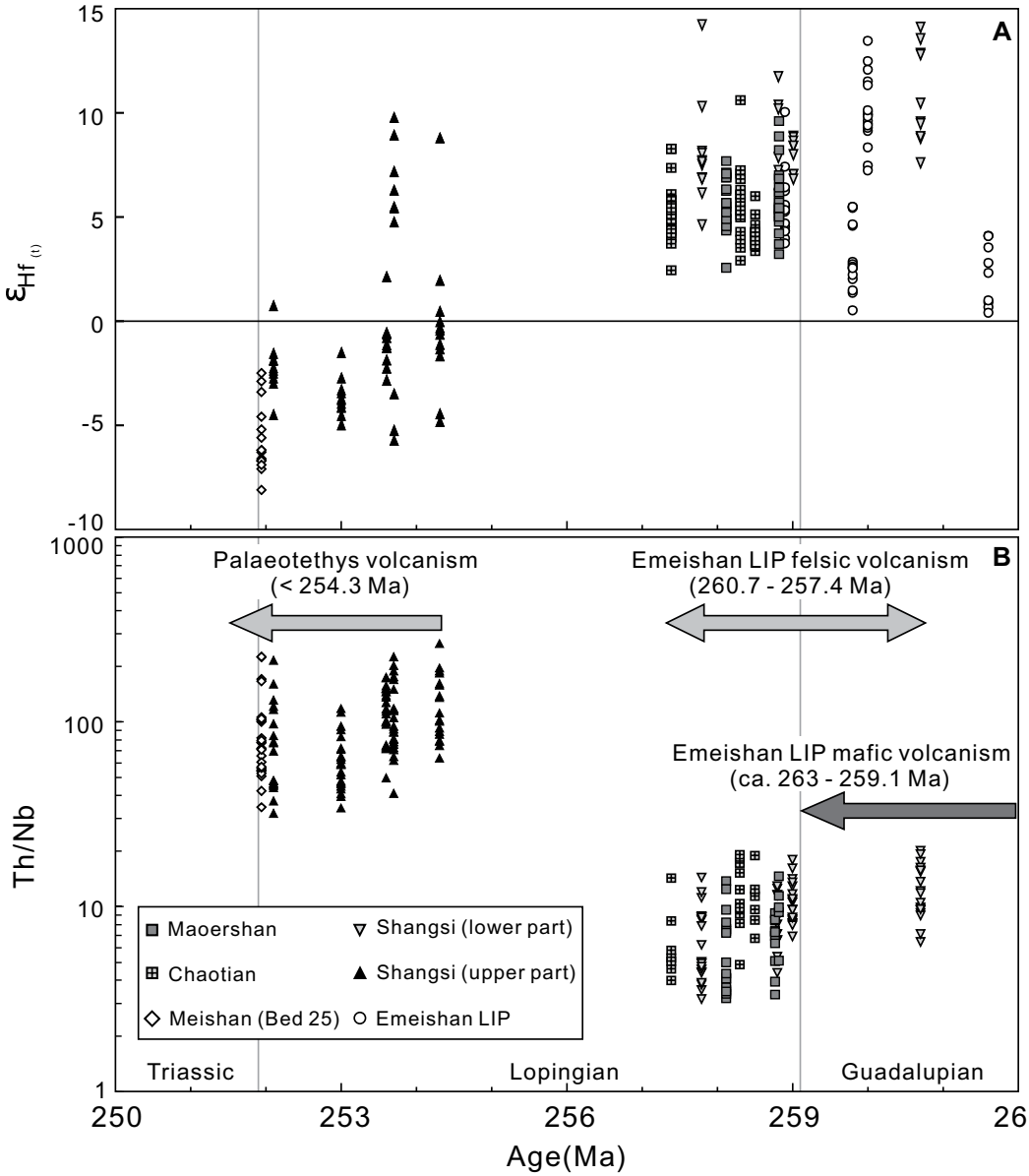

Figure 11. Plots of (A) $\varepsilon_{Hf(t)}$ values versus U-Pb ages and (B) Th/Nb ratios versus U-Pb ages of the zircons from the Maoershan and Chaotian sections. Also shown for comparison are data from the Emeishan large igneous province (LIP) (Xu et al., 2008) and volcanic ash layers from the Shangsi (Shen et al., 2011; Huang et al., 2018) and Meishan sections (Wang et al., 2019).

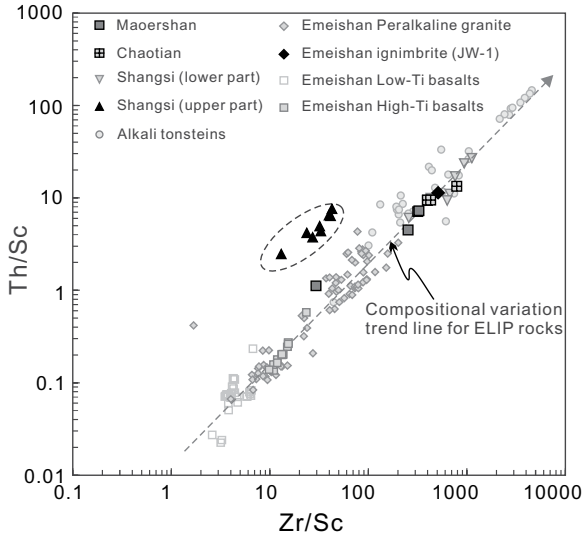

Figure 12. Zr/Sc–Th/Sc diagram (McLennan et al., 1993) of ash samples from the Maoershan and Chaotian sections. Also shown in the plots are ash layers of the Shangsi section (Huang et al., 2018), peralkaline granite (Shellnutt and Zhou, 2007), ignimbrite (Zhong et al., 2014), high-Ti and low-Ti basalts (Xiao et al., 2004) from Emeishan LIP, and Late Permian alkali tonsteins (Dai et al., 2011, 2014b, Zhao et al., 2017). ELIP—Emeishan large igneous province.

phase of the Emeishan LIP occurred between ca. 260.9 Ma and 259.1 Ma, and the earliest eruption occurred at ca. 263.5 Ma. The waning stage of Emeishan volcanism may have lasted until ca. 257.4 Ma in the early Wuchiapingian. Correlating with the timing and duration of faunal turnovers, the end-Guadalupian biotic crisis is shown to have occurred within the duration of the Emeishan LIP volcanism and probably corresponded to the main phase of eruptions (Chen and Xu, 2019). Moreover, the model of proposed drivers focuses on volcanically sourced CO_2, SO_2, and halogens and permits a cause-and-effect relationship between the Emeishan LIP and the end-Guadalupian biotic crisis, although determining the timeline of both events and underlying mechanisms requires further investigation.

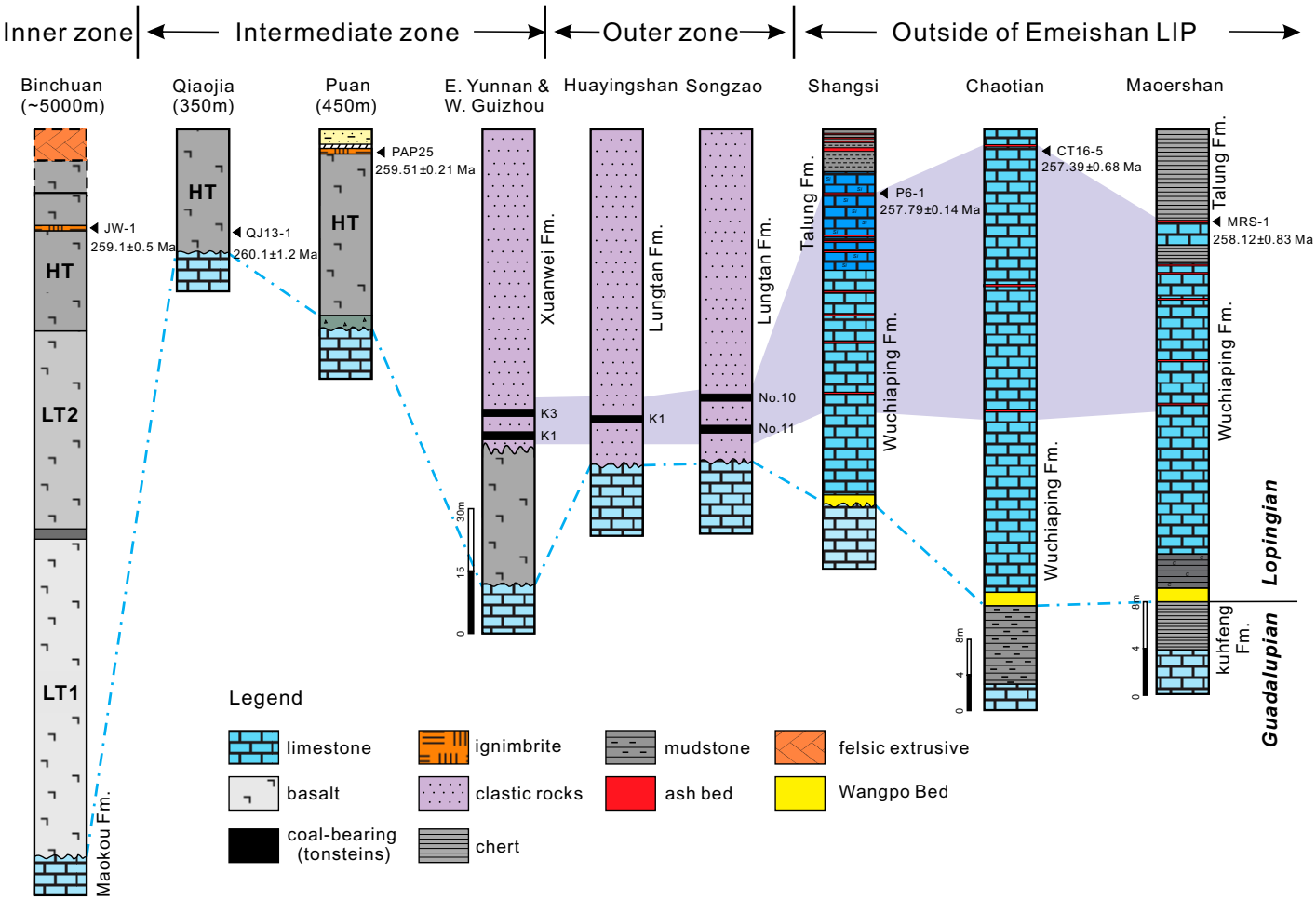

Figure 13. Stratigraphic correlation in the Emeishan LIP and sections studied. Locations of the section are shown in Figure 1A. Data are from Zhong et al. (2014); Li et al. (2018); Yang et al. (2018); Zhao and Graham (2016); Shen et al. (2011); and this study. LIP—large igneous province.

MAIN FINDINGS AND CONCLUSIONS

Our results revealed that the ash layers collected from the early Wuchiapingian are altered volcanic ashes, which were derived from the extrusive alkaline magmatism of the Emeishan LIP. It is reasonable to infer that these ashes are stratigraphically equivalent to the coal-bearing alkali tonsteins in the Xuanwei/Lungtan Formation in southwest China. Moreover, they most likely mark the waning stage of the Emeishan felsic volcanism, which may have continued until ca. 257.4 Ma, equivalent to the upper part of *C. transcaucasica* Zone or the lower part of *C. orientalis* Zone. Also, our interpretation of the distinct provenance change indicates tectonic switching in the source region from the Emeishan LIP to subduction-related magmatism from ca. 257 Ma to ca. 255 Ma.

ACKNOWLEDGMENTS

This research was supported by the Strategic Priority Research Program (B) of the Chinese Academy of Sciences (Grant No. XDB 18000000) and the National Science Foundation of China (Grant nos. 41420104003 and 41403004). We thank the associate editor and two anonymous reviewers for their constructive and insightful reviews, which helped to improve the manuscript. We also acknowledge the effective editorial handling of Science Editor Brad S. Singer. We are very grateful to Lei Zhang, Yingling Hou, Man Wang, and Yizhuo Sun for field assistance. This is contribution IS-2795 from GIGCAS.

REFERENCES CITED

Ali, J.R., Thompson, G.M., Song, X.Y., and Wang, Y.L., 2002, Emeishan Basalts (SW China) and the 'end-Guadalupian' crisis: Magnetobiostratigraphic constraints: Journal of the Geological Society, v. 159, p. 21–29, https://doi.org/10.1144/0016-764901086.

Ali, J.R., Lo, C.H., Thompson, G.M., and Song, X.Y., 2004, Emeishan Basalt Ar-Ar overprint ages define several tectonic events that affected the western Yangtze platform in the Mesozoic and Cenozoic: Journal of Asian Earth Sciences, v. 23, no. 2, p. 163–178, https://doi.org/10.1016/S1367-9120(03)00072-5.

Bagherpour, B., Bucher, H., Schneebeli-Hermann, E., Vennemann, T., Chiaradia, M., and Shen, S.Z., 2018a, Early Late Permian coupled carbon and strontium isotope chemostratigraphy from South China: Extended Emeishan volcanism?: Gondwana Research, v. 58, p. 58–70, https://doi.org/10.1016/j.gr.2018.01.011.

Bagherpour, B., Bucher, H., Yuan, D.X., Leu, M., Zhang, C., and Shen, S.Z., 2018b, Early Wuchiapingian (Lopingian, Late Permian) drowning event in the South China block suggests a late eruptive phase of Emeishan large igneous province: Global and Planetary Change, v. 169, p. 119–132, https://doi.org/10.1016/j.gloplacha.2018.07.013.

Bohor, B.F., and Triplehorn, D.M., 1993, Tonsteins: Altered Volcanic Ash Layers in Coal-bearing Sequences: Geological Society of America Special Paper 285, 44 p.

Bond, D.P.G., Hilton, J., Wignall, P.B., Ali, J.R., Stevens, L.G., Sun, Y.D., and Lai, X.L., 2010, The Middle Permian (Capitanian) mass extinction on land and in the oceans: Earth-Science Reviews, v. 102, p. 100–116, https://doi.org/10.1016/j.earscirev.2010.07.004.

Boven, A., Pasteels, P., Punzalan, L.E., Liu, J., Luo, X., Zhang, W., Guo, Z., and Hertogen, J., 2002, $^{40}Ar/^{39}Ar$ geochronological constraints on the age and evolution of the Permo-Triassic Emeishan volcanic province, southwest China: Journal of Asian Earth Sciences, v. 20, no. 2, p. 157–175, https://doi.org/10.1016/S1367-9120(01)00031-1.

Bryan, S.E., and Ernst, R.E., 2008, Revised definition of large igneous provinces (LIPs): Earth-Science Reviews, v. 86, no. 1-4, p. 175–202, https://doi.org/10.1016/j.earscirev.2007.08.008.

Burger, K., Zhou, Y.P., and Tang, D.H., 1990, Synsedimentary volcanic-ash-derived illite tonsteins in Late Permian coal-bearing formations of southwestern China: International Journal of Coal Geology, v. 15, p. 341–356, https://doi.org/10.1016/0166-5162(90)90071-6.

Burgess, S.D., Bowring, S.A., and Shen, S.Z., 2014, High-precision timeline for Earth's most severe

extinction: Proceedings of the National Academy of Sciences of the United States of America, v. 111, p. 3316–3321, https://doi.org/10.1073/pnas.1317692111.

Burgess, S.D., Bowring, S.A., and Shen, S.Z., 2015, High-precision geochronology confirms voluminous magmatism before, during, and after Earth's most severe extinction: Science Advances, v. 1, p. e1500470, https://doi.org/10.1126/sciadv.1500470.

Cao, C.Q., Cui, C., Chen, J., Summons, R.E., Shen, S.Z., and Zhang, H., 2018, A positive C-isotope excursion induced by sea-level fall in the middle Capitanian of South China: Palaeogeography, Palaeoclimatology, Palaeoecology, v. 505, p. 305–316, https://doi.org/10.1016/j.palaeo.2018.06.010.

Chen, B., Joachimski, M.M., Sun, Y.D., Shen, S.Z., and Lai, X.L., 2011, Carbon and conodont apatite oxygen isotope records of Guadalupian–Lopingian boundary sections: Climatic or sea-level signal?: Palaeogeography, Palaeoclimatology, Palaeoecology, v. 311, p. 145–153, https://doi.org/10.1016/j.palaeo.2011.08.016.

Chen, J., Shen, S.Z., Li, X.H., Xu, Y.G., Joachimski, M.M., Bowring, S.A., Erwin, D.H., Yuan, D.X., Chen, B., Zhang, H., Wang, Y., Cao, C.Q., Zheng, Q.F., and Mu, L., 2016, High-resolution SIMS oxygen isotope analysis on conodont apatite from south China and implications for the end-Permian mass extinction: Palaeogeography, Palaeoclimatology, Palaeoecology, v. 448, p. 26–38, https://doi.org/10.1016/j.palaeo.2015.11.025.

Chen, J., and Xu, Y.G., 2017, Permian large igneous provinces and their impact on paleoenvironment and biodiversity: Progresses and perspectives: Bulletin of Mineralogy [in Chinese with English abstract]: Petrology and Geochemistry, v. 36, p. 374–393.

Chen, J., and Xu, Y.G., 2019, Establishing the link between Permian volcanism and biodiversity changes: Insights from geochemical proxies: Gondwana Research, v. 75, p. 68–96, https://doi.org/10.1016/j.gr.2019.04.008.

Cheng, L.L., Wang, Y., Herrin, J.S., Ren, Z.Y., and Yang, Z.F., 2017, Origin of K-feldspar megacrysts in rhyolites from the Emeishan large igneous province, southwest China: Lithos, v. 294-295, p. 397–411, https://doi.org/10.1016/j.lithos.2017.10.018.

Chung, S.L., and Jahn, B.M., 1995, Plume-lithosphere interaction in generation of the Emeishan flood basalts at the Permian–Triassic boundary: Geology, v. 23, p. 889–892, https://doi.org/10.1130/0091-7613(1995)023<0889:PLIIGO>2.3.CO;2.

Dai, S.F., Wang, X.B., Zhou, Y.P., Hower, J.C., Li, D.H., Chen, W.M., Zhu, X.W., and Zou, J.H., 2011, Chemical and mineralogical compositions of silicic, mafic, and alkali tonsteins in the late Permian coals from the Songzao Coalfield, Chongqing, southwest China: Chemical Geology, v. 282, p. 29–44, https://doi.org/10.1016/j.chemgeo.2011.01.006.

Dai, S.F., Li, T., Seredin, V.V., Ward, C.R., Hower, J.C., Zhou, Y.P., Zhang, M.Q., Song, X.L., Song, W.J., and Zhao, C.L., 2014a, Origin of minerals and elements in the Late Permian coals, tonsteins, and host rocks of the Xinde Mine, Xuanwei, eastern Yunnan, China: International Journal of Coal Geology, v. 121, p. 53–78, https://doi.org/10.1016/j.coal.2013.11.001.

Dai, S.F., Luo, Y.B., Seredin, V.V., Ward, C.R., Hower, J.C., Zhao, L., Liu, S.D., Zhao, C.L., Tian, H.M., and Zou, J.H., 2014b, Revisiting the Late Permian coal from the Huayingshan, Sichuan, southwestern China: Enrichment and occurrence modes of minerals and trace elements: International Journal of Coal Geology, v. 122, p. 110–128, https://doi.org/10.1016/j.coal.2013.12.016.

Dai, S.F., Liu, J.J., Ward, C.R., Hower, J.C., French, D., Jia, S.H., Hood, M.M., and Garrison, T.M., 2016, Mineralogical and geochemical compositions of Late Permian coals and host rocks from the Guxu Coalfield, Sichuan Province, China, with emphasis on enrichment of rare metals: International Journal of Coal Geology, v. 166, p. 71–95, https://doi.org/10.1016/j.coal.2015.12.004.

Dai, S.F., Nechaev, V.P., Chekryzhov, I.Y., Zhao, L.X., Vysotskiy, S.V., Graham, I., Ward, C.R., Ignatiev, A.V., Velivetskaya, T.A., Zhao, L., French, D., and Hower, J.C., 2018, A model for Nb-Zr-REE-Ga enrichment in Lopingian altered alkaline volcanic ashes: Key evidence of H-O isotopes: Lithos, v. 302-303, p. 359–369, https://doi.org/10.1016/j.lithos.2018.01.005.

Deconinck, J.F., Crasquin, S., Bruneau, L., Pellenard, P., Baudin, F., and Feng, Q., 2014, Diagenesis of clay minerals and K-bentonites in Late Permian/Early Triassic sediments of the Sichuan Basin (Chaotian section, Central China): Journal of Asian Earth Sciences, v. 81, p. 28–37, https://doi.org/10.1016/j.jseaes.2013.11.018.

Ganino, C., Arndt, N.T., Zhou, M.F., Gaillard, F., and Chauvel, C., 2008, Interaction of magma with sedimentary wall rock and magnetite ore genesis in the Panzhihua mafic intrusion, SW China: Mineralium Deposita, v. 43, no. 6, p. 677–694, https://doi.org/10.1007/s00126-008-0191-5.

Goto, A., and Tatsumi, Y., 1996, Quantitative analysis of rock samples by an X-ray fluorescence spectrometer (II): The Rigaku Journal, v. 13, p. 20–38.

Grimes, C.B., Wooden, J.L., Cheadle, M.J., and John, B.E., 2015, "Fingerprinting" tectono-magmatic provenance using trace elements in igneous zircon: Contributions to Mineralogy and Petrology, v. 170, p. 46, https://doi.org/10.1007/s00410-015-1199-3.

Hallam, A., and Wignall, P.B., 1999, Mass extinctions and sea-level changes: Earth-Science Reviews, v. 48, p. 217–250, https://doi.org/10.1016/S0012-8252(99)00055-0.

He, B., Xu, Y.G., Chung, S.L., Xiao, L., and Wang, Y.M., 2003, Sedimentary evidence for a rapid, kilometer-scale crustal doming prior to the eruption of the Emeishan flood basalts: Earth and Planetary Science Letters, v. 213, p. 391–405, https://doi.org/10.1016/S0012-821X(03)00323-6.

He, B., Xu, Y.G., Huang, X.L., Luo, Z.Y., Shi, Y.R., Yang, Q.J., and Yu, S.Y., 2007, Age and duration of the Emeishan flood volcanism, SW China: Geochemistry and SHRIMP zircon U-Pb dating of silicic ignimbrites, post-volcanic Xuanwei Formation and clay tuff at the Chaotian section: Earth and Planetary Science Letters, v. 255, p. 306–323, https://doi.org/10.1016/j.epsl.2006.12.021.

He, B., Xu, Y.G., Zhong, Y.T., and Guan, J.P., 2010, The Guadalupian–Lopingian boundary mudstones at Chaotian (SW China) are clastic rocks rather than acidic tuffs: Implication for a temporal coincidence between the end-Guadalupian mass extinction and the Emeishan volcanism: Lithos, v. 119, p. 10–19, https://doi.org/10.1016/j.lithos.2010.06.001.

Hei, H.X., Su, S.G., Wang, Y., Mo, X.X., Luo, Z.H., and Liu, W.G., 2018, Rhyolites in the Emeishan large igneous province (SW China) with implications for plume-related felsic magmatism: Journal of Asian Earth Sciences, v. 164, p. 344–365, https://doi.org/10.1016/j.jseaes.2018.05.032.

Henderson, C.M., Davydiv, V.I., and Wardlaw, B.R., 2012, The Permian period, *in* Gradstein, F.M., Ogg, J.G., Schmitz, M.D., and Ogg, G.M., eds., The Geological Timescale 2012: Amsterdam, Elsevier, v. 2, p. 653–680.

Hoskin, P.W.O., and Schaltegger, U., 2003, The composition of zircon and igneous and metamorphic petrogenesis: Reviews in Mineralogy and Geochemistry, v. 53, p. 27–62, https://doi.org/10.2113/0530027.

Huang, H., Cawood, P.A., Hou, M.C., Ni, S.J., Yang, J.H., Du, Y.S., and Wen, H.G., 2018, Provenance of Late Permian volcanic ash beds in South China: Implications for the age of Emeishan volcanism and its linkage to climate cooling: Lithos, v. 314–315, p. 293–306, https://doi.org/10.1016/j.lithos.2018.06.009.

Isozaki, Y., Yao, J.X., Matsuda, T., Sakai, H., Ji, Z.S., Shimizu, N., Kobayashi, N., Kawahata, H., Nishi, H., Takano, M., and Kubo, T., 2004, Stratigraphy of the Middle–Upper Permian and Lowermost Triassic at Chaotian, Sichuan, China: Record of Late Permian double mass extinction event: Proceedings of the Japan Academy, ser. B, Physical and Biological Sciences, v. 80, p. 10–16, https://doi.org/10.2183/pjab.80.10.

Isozaki, Y., Shimizu, N., Yao, J.X., Jib, Z.S., and Matsuda, T., 2007, End-Permian extinction and volcanism-induced environmental stress: The Permian–Triassic boundary interval of lower-slope facies at Chaotian, South China: Palaeogeography, Palaeoclimatology, Palaeoecology, v. 252, p. 218–238, https://doi.org/10.1016/j.palaeo.2006.11.051.

Isozaki, Y., Yao, J.X., Ji, Z.S., Saitoh, M., Kobayashi, N., and Sakai, H., 2008, Rapid sea-level change in the Late Guadalupian (Permian) on the Tethyan side of South China: Litho- and biostratigraphy of the Chaotian section in Sichuan: Proceedings of the Japan Academy, ser. B, Physical and Biological Sciences, v. 84, p. 344–353, https://doi.org/10.2183/pjab.84.344.

Jian, P., Liu, D.Y., Kröner, A., Zhang, Q., Wang, Y.Z., Sun, X.M., and Zhang, W., 2009, Devonian to Permian plate tectonic cycle of the Paleo–Tethys Orogen in southwest China (II): Insights from zircon ages of ophiolites, arc/back-arc assemblages and within-plate igneous rocks and generation of the Emeishan CFB province: Lithos, v. 113, no. 3-4, p. 767–784, https://doi.org/10.1016/j.lithos.2009.04.006.

Jin, Y.G., Wang, Y., Wang, W., Shang, Q.H., Cao, C.Q., and Erwin, D.H., 2000, Pattern of marine mass extinction near the Permian–Triassic boundary in South China: Science, v. 289, p. 432–436, https://doi.org/10.1126/science.289.5478.432.

Jin, Y.G., Shen, S.Z., Henderson, C.M., Wang, X.D., Wang, W., Wang, Y., Cao, C.Q., and Shang, Q.H., 2006, The Global Stratotype Section and Point (GSSP) for the boundary between the Capitanian and Wuchiapingian Stage (Permian): Episodes: Journal of International Geoscience, v. 29, p. 253–262, https://doi.org/10.18814/epiiugs/2006/v29i4/003.

Jost, A.B., Mundil, R., He, B., Brown, S.T., Altiner, D., Sun, Y.D., DePaolo, D.J., and Payne, J.L., 2014, Constraining the cause of the end-Guadalupian extinction with coupled records of carbon and calcium isotopes: Earth and Planetary Science Letters, v. 396, p. 201–212, https://doi.org/10.1016/j.epsl.2014.04.014.

Lai, X.L., Wang, W., Wignall, P.B., Bond, D.G., Jiang, H.S., Ali, J.R., John, E.H., and Sun, Y.D., 2008, Palaeoenvironmental change during the end-Guadalupian (Permian) mass extinction in Sichuan, China: Palaeogeography, Palaeoclimatology, Palaeoecology, v. 269, p. 78–93, https://doi.org/10.1016/j.palaeo.2008.08.005.

Li, H.B., Zhang, Z.C., Santosh, M., Lu, L.S., Han, L., and Liu, W., 2017, Late Permian basalts in the Yanghe area, eastern Sichuan Province, SW China: Implications for the geodynamics of the Emeishan flood basalt province and Permian global mass extinction: Journal of Asian Earth Sciences, v, 134, p. 293–308, https://doi.org/10.1016/j.jseaes.2016.11.029.

Li, X.H., Li, Z.X., Zhou, H.W., Liu, Y., and Kinny, P.D., 2002, U-Pb zircon geochronology, geochemistry and Nd isotopic study of Neoproterozoic bimodal volcanic rocks in the Kangdian Rift of South China: Implications for the initial rifting of Rodinia: Precambrian Research, v. 113, p. 135–154, https://doi.org/10.1016/S0301-9268(01)00207-8.

Li, Y.J., He, H.Y., Ivanov, A.V., Demonterova, E.I., Pan, Y.X., Deng, C.L., Zheng, D.W., and Zhu, R.X., 2018, $^{40}Ar/^{39}Ar$ age of the onset of high-Ti phase of the Emeishan volcanism strengthens the link with the end-Guadalupian mass extinction: International Geology Review, v. 60, no. 15, p. 1906–1917, https://doi.org/10.1080/00206814.2017.1405748.

Lin, T.H., Chung, S.L., Chiu, H.Y., Wu, F.Y., Yeh, M.W., Searle, M.P., and Iizuka, Y., 2012, Zircon U–Pb and Hf isotope constraints from the Ailao Shan–Red River shear zone on the tectonic and crustal evolution of southwestern China: Chemical Geology, v. 291, p. 23–37, https://doi.org/10.1016/j.chemgeo.2011.11.011.

Liu, X.J., Liang, Q.D., Li, Z.L., Castillo, P.R., Shi, Y., Xu, J.F., Huang, X.L., Liao, S., Huang, W.L., and Wu, W.N., 2017, Origin of Permian extremely high Ti/Y mafic lavas and dykes from western Guangxi, SW China: Implications for the Emeishan mantle plume magmatism: Journal of Asian Earth Sciences, v. 141, p. 97–111, https://doi.org/10.1016/j.jseaes.2016.09.005.

Lo, C.H., Chung, S.L., Lee, T.Y., and Wu, G.Y., 2002, Age of the Emeishan flood magmatism and relations to Permian–Triassic boundary events: Earth and Planetary Science Letters, v. 198, p. 449–458, https://doi.org/10.1016/S0012-821X(02)00535-6.

Lu, Y.H., 1956, The Permian of Liangshan and its bearing on the classification and correlation of the Permian rocks of South China [in Chinese with English abstract]: Scientia Sinica, v. 5, p. 733–761.

McLennan, S.M., Hemming, S., McDaniel, D.K., and Hanson, G.N., 1993, Geochemical approaches to

sedimentation, provenance, and tectonics, *in* Johnsson, M.J., and Basu, A., eds., Processes Controlling the Composition of Clastic Sediments: Geological Society of America Special Paper 284, p. 21–40, https://doi.org/10.1130/SPE284-p21.

Mei, S.L., Jin, Y.G., and Wardlaw, B.R., 1998, Conodont succession of the Guadalupian–Lopingian boundary strata in Laibin of Guangxi, China and west Texas, USA: Palaeoworld, v. 9, p. 53–76.

Metcalfe, I., 1996, Pre-Cretaceous evolution of SE Asian terranes: Geological Society, London, Special Publications 106, no. 1, p. 97–122, https://doi.org/10.1144/GSL.SP.1996.106.01.09.

Metcalfe, I., 2011, Palaeozoic–Mesozoic History of SE Asia: Geological Society, London, Special Publication 355, no. 1, p. 7–35, https://doi.org/10.1144/SP355.2.

Mundil, R., Metcalfe, I., Ludwig, K.R., Renne, P.R., Oberli, F., and Nicoll, R.S., 2001, Timing of the Permian–Triassic biotic crisis: Implications from new zircon U/Pb age data (and their limitations): Earth and Planetary Science Letters, v. 187, p. 131–145, https://doi.org/10.1016/S0012-821X(01)00274-6.

Mundil, R., Ludwig, K.R., Metcalfe, I., and Renne, P.R., 2004, Age and timing of the Permian mass extinctions: U/Pb dating of closed-system zircons: Science, v. 305, p. 1760–1763, https://doi.org/10.1126/science.1101012.

Ogg, J.G., Ogg, G., and Gradstein, F.M., 2016, A Concise Geologic Time Scale: Amsterdam, Elsevier, p. 123–124.

Pearce, J.A., and Peate, D.W., 1995, Tectonic implications of the composition of volcanic arc magmas: Annual review of Earth and planetary sciences, v. 23, no. 1, p. 251–285, https://doi.org/10.1146/annurev.ea.23.050195.001343.

Xiao, L., Xu, Y.G., Mei, H.J., Zheng, Y.F., He, B., and Pirajno, F., 2004, Distinct mantle sources of low-Ti and high-Ti basalts from the western Emeishan large igneous province, SW China: implications for plume–lithosphere interaction: Earth and Planetary Science Letters, v. 228, no. 3-4, p. 525–546, https://doi.org/10.1016/j.epsl.2004.10.002.

Saitoh, M., Isozaki, Y., Ueno, Y., Yoshida, N., Yao, J., and Ji, Z., 2013a, Middle–Upper Permian carbon isotope stratigraphy at Chaotian, South China: Pre-extinction multiple upwelling of oxygen-depleted water onto continental shelf: Journal of Asian Earth Sciences, v. 67–68, p. 51–62, https://doi.org/10.1016/j.jseaes.2013.02.009.

Saitoh, M., Isozaki, Y., Yao, J., Ji, Z., Ueno, Y., and Yoshida, N., 2013b, The appearance of an oxygen-depleted condition on the Capitanian disphotic slope/basin in South China: Middle–Upper Permian stratigraphy at Chaotian in northern Sichuan: Global and Planetary Change, v. 105, p. 180–192, https://doi.org/10.1016/j.gloplacha.2012.01.002.

Shellnutt, J.G., 2014, The Emeishan large igneous province: A synthesis: Geoscience Frontiers, v. 5, p. 369–394, https://doi.org/10.1016/j.gsf.2013.07.003.

Shellnutt, J.G., and Zhou, M.F., 2007, Permian peralkaline, peraluminous and metaluminous A-type granites in the Panxi district, SW China: Their relationship to the Emeishan mantle plume: Chemical Geology, v. 243, p. 286–316, https://doi.org/10.1016/j.chemgeo.2007.05.022.

Shellnutt, J.G., Jahn, B.M., and Zhou, M.F., 2011, Crustally derived granites in the Panzhihua region, SW China: Implications for felsic magmatism in the Emeishan large igneous province: Lithos, v. 123, p. 145–157, https://doi.org/10.1016/j.lithos.2010.10.016.

Shellnutt, J.G., Denyszyn, S.W., and Mundil, R., 2012, Precise age determination of mafic and felsic intrusive rocks from the Permian Emeishan large igneous province (SW China): Gondwana Research, v. 22, p. 118–126, https://doi.org/10.1016/j.gr.2011.10.009.

Shen, S.Z., and Shi, G.R., 2002, Paleobiogeographical extinction patterns of Permian brachiopods in the Asian-western Pacific region: Paleobiology, v. 28, no. 4, p. 449–463, https://doi.org/10.1666/0094-8373(2002)028<0449:PEPOPB>2.0.CO;2.

Shen, S.Z., Henderson, C.M., Bowring, S.A., Cao, C.Q., Wang, Y., Wang, W., Zhang, H., Zhang, Y.C., and Mu, L., 2010, High-resolution Lopingian (Late Permian) timescale of South China: Geological Journal, v. 45, p. 122–134, https://doi.org/10.1002/gj.1232.

Shen, S.Z., Crowley, J.L., Wang, Y., Bowring, S.A., Erwin, D.H., Sadler, P.M., Cao, C.Q., Rothman, D.H., Henderson, C.M., Ramezani, J., Zhang, H., Shen, Y.N., Wang, X.D., Wang, W., Mu, L., Li, W.Z., Tang, Y.G., Liu, X.L., Liu, L.J., Zeng, Y., Jiang, Y.F., and Jin, Y.G., 2011, Calibrating the end-Permian mass extinction: Science, v. 334, p. 1367–1372, https://doi.org/10.1126/science.1213454.

Shen, S.Z., Ramezani, J., Chen, J., Cao, C.Q., Erwin, D.H., Zhang, H., Xiang, L., Schoepfer, S.D., Henderson, C.M., Zheng, Q.F., Bowring, S.A., Wang, Y., Li, X.H., Wang, X.D., Yuan, D.X., Zhang, Y.C., Mu, L., Wang, J., and Wu, Y.S., 2019a, A sudden end-Permian mass extinction in South China: Geological Society of America Bulletin, v. 131, p. 205–223, https://doi.org/10.1130/B31909.1.

Shen, S.Z., Zhang, H., Zhang, Y.C., Yuan, D.X., Chen, B., He, W.H., Mu, L., Lin, W., Wang, W.Q., Chen, J., Wu, Q., Cao, C.Q., Wang, Y., and Wang, X.D., 2019b, Permian integrative stratigraphy and timescale of China: Science China: Earth Sciences, v. 62, p. 154–188, https://doi.org/10.1007/s11430-017-9228-4.

Sone, M., and Metcalfe, I., 2008, Parallel Tethyan sutures in mainland Southeast Asia: New insights for Palaeo–Tethys closure and implications for the Indosinian orogeny: Comptes Rendus Geoscience, v. 340, no. 2-3, p. 166–179, https://doi.org/10.1016/j.crte.2007.09.008.

Song, H.J., Wignall, P.B., Tong, J.N., and Yin, H.F., 2013, Two pulses of extinction during the Permian–Triassic crisis: Nature Geoscience, v. 6, p. 52–56, https://doi.org/10.1038/ngeo1649.

Spears, D.A., 2012, The origin of tonsteins, an overview, and links with seatearths, fireclays and fragmental clay rocks: International Journal of Coal Geology, v. 94, p. 22–31, https://doi.org/10.1016/j.coal.2011.09.008.

Sun, S.S., and McDonough, W.F., 1989, Chemical and Isotopic Systematics of Oceanic Basalts: Implications for Mantle Composition and Processes: Geological Society, London, Special Publication 42, p. 313–345, https://doi.org/10.1144/GSL.SP.1989.042.01.19.

Sun, Y.D., Lai, X.L., Wignall, P.B., Widdowson, M., Ali, J.R., Jiang, H.S., Wang, W., Yan, C.B., Bond, D.P.G., and Vedrine, S., 2010, Dating the onset and nature of the Middle Permian Emeishan large igneous province eruptions in SW China using conodont biostratigraphy and its bearing on mantle plume uplift models: Lithos, v. 119, p. 20–33, https://doi.org/10.1016/j.lithos.2010.05.012.

Sun, Y.D., Liu, X.T., Yan, J.X., Li, B., Chen, B., Bond, D.P.G., Joachimski, M.M., Wignall, P.B., Wang, X., and Lai, X.L., 2017, Permian (Artinskian to Wuchapingian) conodont biostratigraphy in the Tieqiao section, Laibin area, South China: Palaeogeography, Palaeoclimatology, Palaeoecology, v. 465, p. 42–63, https://doi.org/10.1016/j.palaeo.2016.10.013.

Usuki, T., Lan, C.Y., Tran, T.H., Pham, T.D., Wang, K.L., Shellnutt, G.J., and Chung, S.L., 2015, Zircon U-Pb ages and Hf isotopic compositions of alkaline silicic magmatic rocks in the Phan Si Pan–Tu Le region, northern Vietnam: Identification of a displaced western extension of the Emeishan Large Igneous Province: Journal of Asian Earth Sciences, v. 97, p. 102–124, https://doi.org/10.1016/j.jseaes.2014.10.016.

Wang, G.Q., 2004, Late Permian eustatic fluctuation in north part of central Yangtze Platform and its influence on biotic crisis events [Ph.D. thesis]: Wuhan, China University of Geosciences, 97 p.

Wang, X.D., Cawood, P.A., Zhao, L.S., Chen, Z.Q., Lyu, Z.Y., and Ma, B., 2019, Convergent continental margin volcanic source for ash beds at the Permian–Triassic boundary, South China: Constraints from trace elements and Hf-isotopes: Palaeogeography, Palaeoclimatology, Palaeoecology, v. 519, p. 154–165, https://doi.org/10.1016/j.palaeo.2018.02.011.

Wang, Y., and Jin, Y.G., 2000, Permian palaeogeographic evolution of the Jiangnan Basin, South China: Palaeogeography, Palaeoclimatology, Palaeoecology, v. 160, p. 35–44, https://doi.org/10.1016/S0031-0182(00)00043-2.

Wang, Y.J., Qian, X., Cawood, P.A., Liu, H.C., Feng, Q.L., Zhao, G.C., Zhang, Y.H., He, H.Y., and Zhang, P.Z., 2018, Closure of the East Paleotethyan Ocean and amalgamation of the Eastern Cimmerian and Southeast Asia continental fragments: Earth-Science Reviews, v. 186, p. 195–230, https://doi.org/10.1016/j.earscirev.2017.09.013.

Wignall, P.B., Sun, Y.D., Bond, D.P.G., Izon, G., Newton, R.J., Vedrine, S., Widdowson, M., Ali, J.R., Lai, X.L., Jiang, H.S., Cope, H., and Bottrell, S.H., 2009, Volcanism, mass extinction, and carbon isotope fluctuations in the Middle Permian of China: Science, v. 324, p. 1179–1182, https://doi.org/10.1126/science.1171956.

Winchester, J.A., and Floyd, P.A., 1977, Geochemical discrimination of different magma series and their differentiation products using immobile elements: Chemical Geology, v. 20, p. 325–343, https://doi.org/10.1016/0009-2541(77)90057-2.

Xu, Y.G., and He, B., 2007, Thick and high velocity crust in Emeishan large igneous province, SW China: Evidence for crustal growth by magmatic underplating/intraplating, *in* Foulger, G., and Jurdy, D., eds., The Origins of Melting Anomalies: Plates, Plumes, and Planetary Processes: Geological Society of America Special Publication 430, p. 841–858.

Xu, Y.G., Chung, S.L., Jahn, B.M., and Wu, G.Y., 2001, Petrologic and geochemical constraints on the petrogenesis of Permian–Triassic Emeishan flood basalts in southwestern China: Lithos, v. 58, p. 145–168, https://doi.org/10.1016/S0024-4937(01)00055-X.

Xu, Y.G., Luo, Z.Y., Huang, X.L., He, B., Xiao, L., Xie, L.W., and Shi, Y.R., 2008, Zircon U–Pb and Hf isotope constraints on crustal melting associated with the Emeishan mantle plume: Geochimica et Cosmochimica Acta, v. 72, p. 3084–3104, https://doi.org/10.1016/j.gca.2008.04.019.

Xu, Y.G., Chung, S.L., Shao, H., and He, B., 2010, Silicic magmas from the Emeishan large igneous province, southwest China: Petrogenesis and their link with the end-Guadalupian biological crisis: Lithos, v. 119, p. 47–60, https://doi.org/10.1016/j.lithos.2010.04.013.

Yang, J.H., Cawood, P.A., Du, Y.S., Huang, H., Huang, H.W., and Tao, P., 2012, Large Igneous Province and magmatic arc sourced Permian–Triassic volcanogenic sediments in China: Sedimentary Geology, v. 261-262, p. 120–131, https://doi.org/10.1016/j.sedgeo.2012.03.018.

Yang, J.H., Cawood, P.A., and Du, Y.S., 2015, Voluminous silicic eruptions during Late Permian Emeishan igneous province and link to climate cooling: Earth and Planetary Science Letters, v. 432, p. 166–175, https://doi.org/10.1016/j.epsl.2015.09.050.

Yang, J.H., Cawood, P.A., Du, Y.S., Condon, D.J., Yan, J.X., Liu, J.Z., Huang, Y., and Yuan, D.X., 2018, Early Wuchiapingian cooling linked to Emeishan basaltic weathering?: Earth and Planetary Science Letters, v. 492, p. 102–111, https://doi.org/10.1016/j.epsl.2018.04.004.

Yuan, D.X., Shen, S.Z., Henderson, C.M., Chen, J., Zhang, H., Zheng, Q.F., and Wu, H.C., 2019, Integrative timescale for the Lopingian (Late Permian): A review and update from Shangsi, south China: Earth-Science Reviews, v. 188, p. 190–209, https://doi.org/10.1016/j.earscirev.2018.11.002.

Zhang, L.L., Zhang, N., and Xia, W.C., 2007, Conodont succession in the Guadalupian–Lopingian boundary interval (upper Permian) of the Maoershan section, Hubei Province, China: Micropaleontology, v. 53, p. 433–446, https://doi.org/10.2113/gsmicropal.53.6.433.

Zhang, Y., Ren, Z.Y., and Xu, Y.G., 2013, Sulfur in olivine-hosted melt inclusions from the Emeishan picrites: Implications for S degassing and its impact on environment: Journal of Geophysical Research: Solid Earth, v. 118, p. 4063–4070, https://doi.org/10.1002/jgrb.50324.

Zhao, L., and Graham, I., 2016, Origin of the alkali tonsteins from southwest China: Implications for alkaline magmatism associated with the waning stages of the Emeishan Large Igneous Province: Australian Journal of Earth Sciences, v. 63, no. 1, p. 123–128, https://doi.org/10.1080/08120099.2016.1133456.

Zhao, L., Dai, S., Graham, I.T., Li, X., Liu, H., Song, X., Hower, J.C., and Zhou, Y., 2017, Cryptic sediment-hosted critical element mineralization from eastern

Yunnan Province, southwestern China: Mineralogy, geochemistry, relationship to Emeishan alkaline magmatism and possible origin: Ore Geology Reviews, v. 80, p. 116–140, https://doi.org/10.1016/j.oregeorev.2016.06.014.

Zhong, Y.T., He, B., Mundil, R., and Xu, Y.G., 2014, CA–TIMS zircon U-Pb dating of felsic ignimbrite from the Binchuan section: Implications for the termination age of Emeishan large igneous province: Lithos, v. 204, p. 14–19, https://doi.org/10.1016/j.lithos.2014.03.005.

Zhou, M.F., Malpas, J., Song, X.Y., Robinson, P.T., Sun, M., Kennedy, A.K., Lesher, C.M., and Keays, R.R., 2002, A temporal link between the Emeishan large igneous province (SW China) and the end-Guadalupian mass extinction: Earth and Planetary Science Letters, v. 196, p. 113–122, https://doi.org/10.1016/S0012-821X(01)00608-2.

Zhou, Y.P., 1999, The synsedimentary alkalinity-volcanic ash derived tonsteins of early Longtan age in southwestern China: Coal Geology and Exploration, v. 27, p. 5–9.

Zhou, Y.P., Ren, Y., and Bohor, B.F., 1982, Origin and distribution of tonsteins in Late Permian coal seams of southwestern China: International Journal of Coal Geology, v. 2, p. 49–77, https://doi.org/10.1016/0166-5162(82)90015-5.

Zhou, Y.P., Bohor, B.F., and Ren, Y., 2000, Trace element geochemistry of altered volcanic ash layers (tonsteins) in Late Permian coal-bearing formations of eastern Yunnan and western Guizhou Provinces, China: International Journal of Coal Geology, v. 44, p. 305–324, https://doi.org/10.1016/S0166-5162(00)00017-3.

Zi, J.W., Cawood, P.A., Fan, W.M., Tohver, E., Wang, Y.J., McCuaig, T.C., and Peng, T.P., 2013, Late Permian–Triassic magmatic evolution in the Jinshajiang orogenic belt, SW China and implications for orogenic processes following closure of the Paleo–Tethys: American Journal of Science, v. 313, no. 2, p. 81–112, https://doi.org/10.2475/02.2013.02.

Science Editor: Bradley S. Singer
Associate Editor: William Clyde

Manuscript Received 17 August 2019
Revised Manuscript Received 21 November 2019
Manuscript Accepted 7 January 2020

Printed in the USA